REPORT 1038

WIND-TUNNEL INVESTIGATION OF AIR INLET AND OUTLET OPENINGS ON A STREAMLINE BODY[1]

By John V. Becker

SUMMARY

In connection with the general problem of providing air flow to an aircraft power plant located within a fuselage, an investigation was conducted in the Langley 8-foot high-speed tunnel to determine the effect on external drag and pressure distribution of air inlet openings located at the nose of a streamline body. Air outlet openings located at the tail and at the 21-percent and 63-percent stations of the body were also investigated. Boundary-layer transition measurements were made and correlated with the force and the pressure data. Individual openings were investigated with the aid of a blower and then practicable combinations of inlet and outlet openings were tested. Various modifications to the internal duct shape near the inlet opening and the aerodynamic effects of a simulated gun in the duct were also studied.

The results showed that the external drag (measured drag less computed drag due to internal duct losses) of the body with suitably designed nose-inlet and tail-outlet openings was no higher than the drag of the streamline body over a wide range of rates of internal air flow. The static-pressure distribution with the best inlet profiles developed during the investigation was almost identical with that of the corresponding portion of the streamline body. As a consequence, the same favorable laminar-boundary-layer flow as on the streamline body was obtained. The local velocity increments over the nose profiles were so low that the critical speed of a fuselage employing these shapes would depend on the peak-velocity increments occurring elsewhere than on the nose.

The results of the tests suggested that outlet openings should be designed so that the static pressure of the internal flow at the outlet would be the same as the static pressure of the external flow in the vicinity of the opening. Radical changes in the internal-duct arrangement near the inlet openings had little effect on the external drag or pressure distribution.

INTRODUCTION

Various wind-tunnel tests of full-scale airplanes and of airplane models have shown large external losses associated with the power-plant installations. The external drag of clean NACA cowling installations with no protruding scoops or surface irregularities was shown in reference 1 to be considerable. At high speeds, prohibitive increases in the external drag may occur as a result of the formation of compression shocks on cowlings (reference 2) or protruding scoops. The excessive cowling drag costs at high speeds can be reduced to some extent by reducing the bluntness of the nose profile (reference 2); however, the improvement which can be made in this direction is limited for conventional installations in which the engine is located at the nose of the fuselage. If it is assumed that the engine is located near the center of the fuselage or nacelle, then radical changes in the shape of the nose are possible. The present investigation was designed to explore the possibilities of high-speed drag reduction by use of nose inlets proportioned solely from aerodynamic requirements without any restrictions arising from engine dimensions, location, or air-flow requirements.

At the outset of the present investigation little information was available in regard to the characteristics of inlet openings at the nose of a streamline body. Previous tests had been made without air flow into the openings, a condition seldom occurring in practice, and the results were therefore inconclusive. Little pressure-distribution or critical-speed data were available, and it was not known whether any appreciable laminar boundary layer could exist behind an inlet opening.

The principal purpose of this investigation was to develop nose-inlet openings of various relative sizes which would have the lowest possible external drag and the highest possible critical compressibility speed. The air-inlet flow rates used were not restricted to the relatively small requirements of radial engines but were varied from zero flow to inlet-velocity ratios in excess of unity. Pressure-distribution and boundary-layer data were obtained to aid in interpreting the drag results and to permit the estimation of the critical speeds. Typical annular and tail-outlet openings were similarly investigated. In order to avoid possible confusing interference effects, the inlet and the outlet openings were tested separately with the internal air flow being supplied through wing ducts from a blower located outside of the wind tunnel. Representative combinations of the inlet and outlet openings were then tested without the use of the blower. The effects on external drag of a protruding simulated gun in the inlet opening and of various internal-duct arrangements near the nose were also included in the investigation of the individual inlet openings.

[1] Supersedes NACA ACR, "Wind-Tunnel Tests of Air Inlet and Outlet Openings on a Streamline Body" by John V. Becker, November 1940.

The external drag cost of an inlet opening at the nose of a smooth streamline body is generally greater at low Reynolds numbers, when the opening may disturb extensive low-drag laminar boundary layers, than at high-speed flight Reynolds numbers, where the boundary-layer flow may be almost wholly turbulent. Although it was impossible to attain full-scale conditions in this investigation, the boundary-layer-flow condition corresponding to high Reynolds numbers was simulated by artificially forcing transition to take place near the nose of the models. The tests were made both with the natural-transition and the fixed-transition boundary-layer conditions. The results thus show the effect of the openings at conditions corresponding to extremes of the Reynolds number range.

SYMBOLS

V	free-stream velocity
p_0	free-stream static pressure
ρ_0	free-stream density
q_0	free-stream dynamic pressure $\left(\frac{1}{2}\rho_0 V^2\right)$
v	mean velocity in duct
p	local static pressure
ρ	density in duct
V_i	initial velocity of air passing through duct
V_w	hypothetical final velocity of air passing through duct based on total pressure at discharge
A	cross-sectional area of inlet or outlet opening
d	diameter of inlet or outlet opening
D	maximum diameter of streamline body
F	maximum cross-sectional area of streamline body
L	length of streamline body
l	distance between end of streamline body and end of nose
R	maximum radius of streamline body
R	fuselage Reynolds number (VL/ν)
ν	kinematic viscosity
P	pressure coefficient $((p-p_0)/q_0)$
a	velocity of sound in air
M	Mach number (V/a)
Q	volume of flow through duct, cubic feet per second
α	angle of attack referred to center line of streamline body, degrees
C_{D_F}	external-drag coefficient $\left(\frac{\left[\text{(Measured drag of model)}-\text{(Drag of wing alone)}-\text{(Drag due to internal flow)}\right]}{q_0 F}\right)$
$C_{D_{Fi}}$	calculated drag coefficient due to internal air flow
U	velocity just outside the boundary layer
u	velocity in the boundary layer
x	distance from nose of streamline body, along major axis
x'	distance from nose of inlet openings, along major axis
X	length of nose measured from $L/4$ station
y	ordinate measured from center line of streamline body
y'	nose-profile ordinate measured from inlet-opening radius
Y	value of y' at $L/4$ station

APPARATUS AND METHODS

The tests were made in the Langley 8-foot high-speed tunnel in its original form incorporating an 8,000-horsepower drive motor. The tunnel was of the closed-throat, circular-section, single-return type and was capable of air speeds of about 500 miles per hour at the time of these tests. This tunnel was chosen for the investigation principally because of the low turbulence of the air stream, which permitted the boundary-layer-flow conditions more nearly to approach those obtained in free air than in streams of high turbulence. Most of the tests were run at low speed (140 miles per hour).

Streamline body.—The streamline body (fig. 1 and table I) is a slightly modified version of fuselage form No. 111 of reference 3. The thickness distribution was modified slightly to eliminate the unfavorable pressure gradient occurring ahead of the 50-percent station of the original 111 form. This modification was made to encourage a more extensive laminar boundary layer. The fineness ratio of 5 is representative of several current pursuit-type fuselages.

The streamline body was mounted in the wind tunnel on a 24-inch-chord airfoil of NACA 27-212 section, which completely spanned the jet (fig. 2). The wing contained two large ducts to permit air to be supplied to or drawn from the openings on the body. The ratio of wing chord at the body to the length of the body is within the range of current practice.

Inlet openings.—Nose-inlet openings of three sizes were tested (figs. 1 and 3; ordinates in table I). The largest opening, nose A, was approximately the size, relative to the maximum cross section of the body, of average NACA cowling

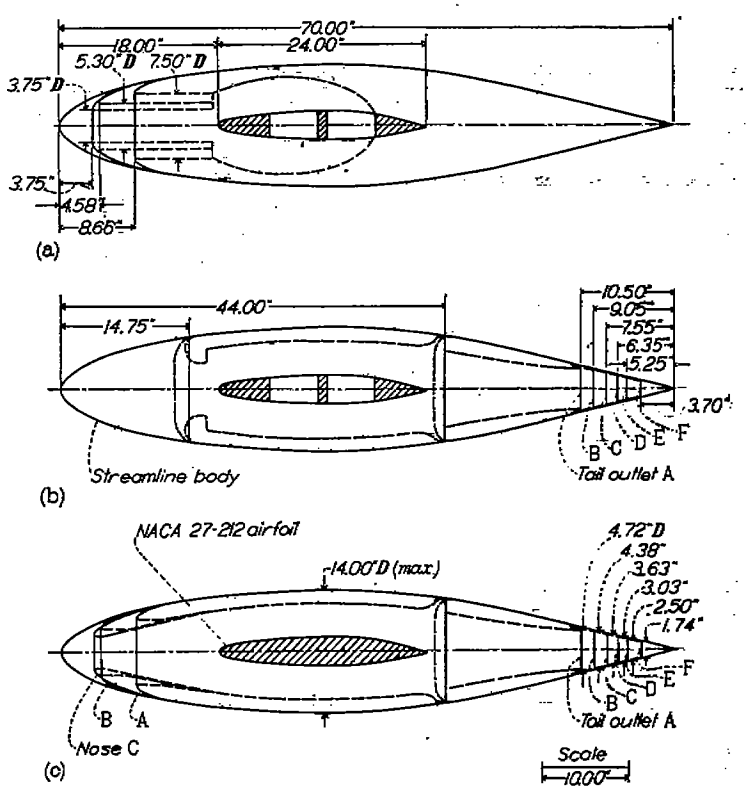

(a) Inlet openings.
(b) Outlet openings.
(c) Inlet-outlet combinations.

FIGURE 1.—Streamline body with general arrangement of inlet and outlet openings

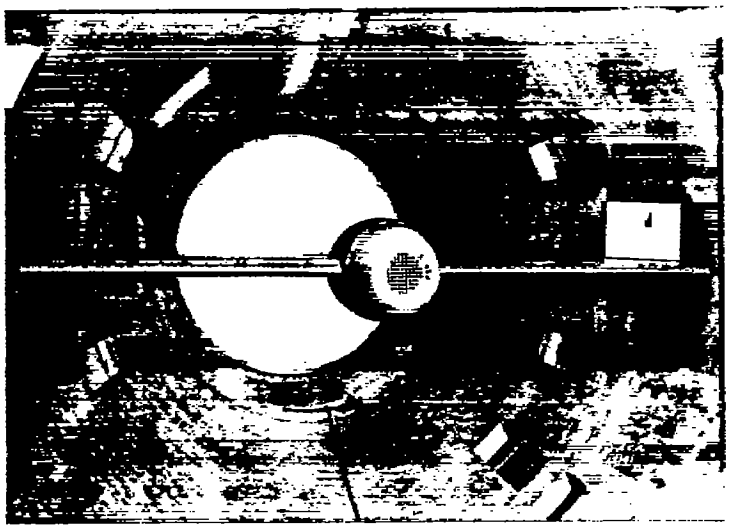

FIGURE 2.—Model installed in Langley 8-foot high-speed tunnel. Nose B.

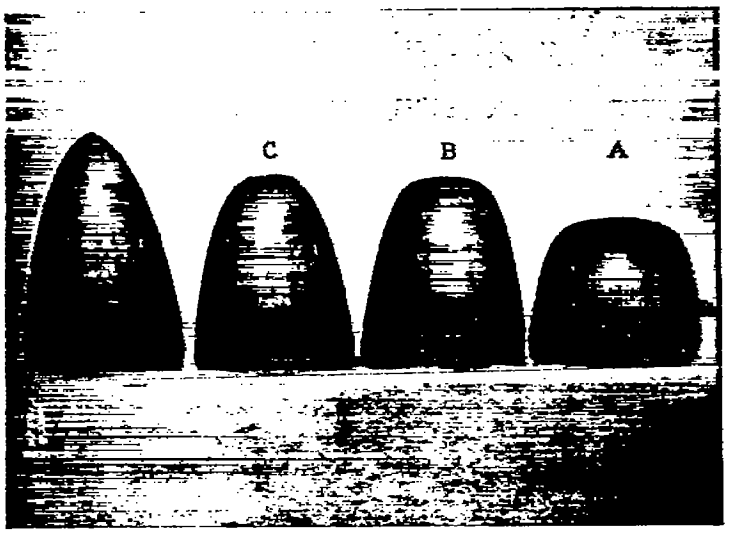

FIGURE 3.—Nose inlet openings compared with streamline nose.

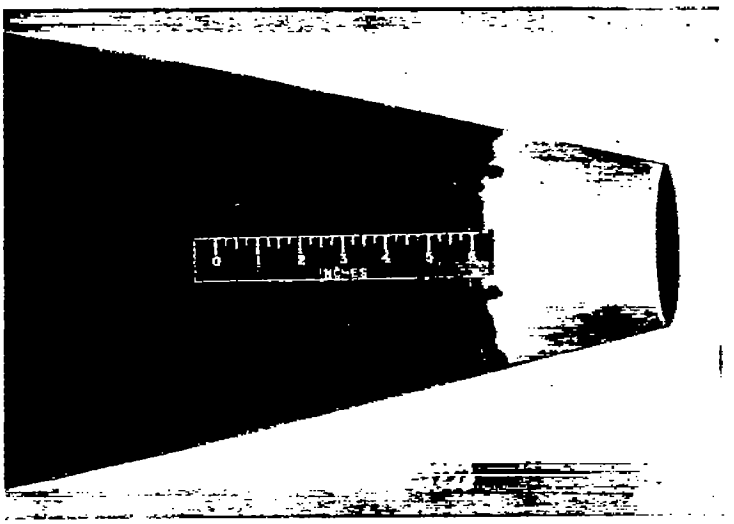

FIGURE 4.—Typical tail outlet opening. Tail C.

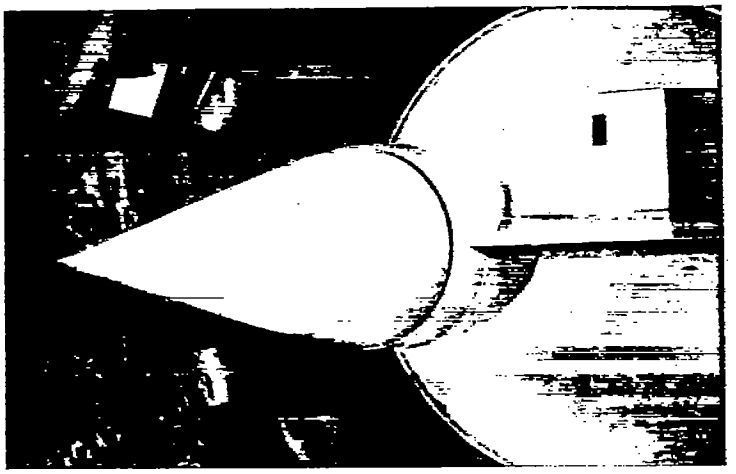

FIGURE 5.—Annular outlet opening at $x=0.63L$.

inlet openings. Nose B had one-half the area of nose A, and nose C, one-quarter the area of nose A. The profile shapes of the noses were developed in a series of tests (not discussed in detail in this report) in which the nose lengths and profiles were progressively modified until the most satisfactory pressure-distribution characteristics were obtained. The profiles all fall within the profile of the streamline body. It will be noticed that the nose ordinates (table I) are given only to the quarter-length station. Beyond this point, streamline-body ordinates apply. Several modifications of the straight duct (fig. 1) that was used in most of the nose-inlet tests will be described later in the discussion of the results.

Outlet openings.—Outlet openings at the tail and annular outlets located ahead of and behind the wing were investigated (figs. 1, 4, and 5). The tail-outlet profiles coincide with the streamline-body lines. Various tail-outlet areas were obtained by successively decreasing the length of the body. The internal duct was of converging section to represent typical practice in the design of outlet openings. The annular outlet openings were designed primarily to exhaust the air as nearly as possible in the stream direction. The areas were selected from consideration of the quantity of air required by a radial engine large enough to occupy the maximum section of a fuselage. The outlet openings are not in any sense optimum shapes arrived at on the basis of experiment as in the case of the inlet openings; they merely represent typical design practice.

Blower setup.—Air flow in the tests of the individual openings was supplied by a 50-horsepower centrifugal blower mounted outside the wind tunnel on the floor of the test chamber (figs. 6 and 7). Freedom of the floating balance structure was maintained by a mercury seal that connected the blower duct to the wing duct leading to the model. The air flow through the mercury seal was at right angles to the longitudinal (drag) axis of the wind tunnel so that the flow had no momentum in the drag direction. Preliminary tests were made throughout the range of blower speeds at zero air speed in the tunnel, with and without air inlet, to insure that the pressures and flow at the mercury seal had no effect on the drag scale readings.

The flow was metered by a venturi installed on the balance ring between the mercury seal and the model. Several calibrations were made with the venturi in its operating position by surveying the flow in the duct with a rake of 25 total-pressure and 7 static tubes.

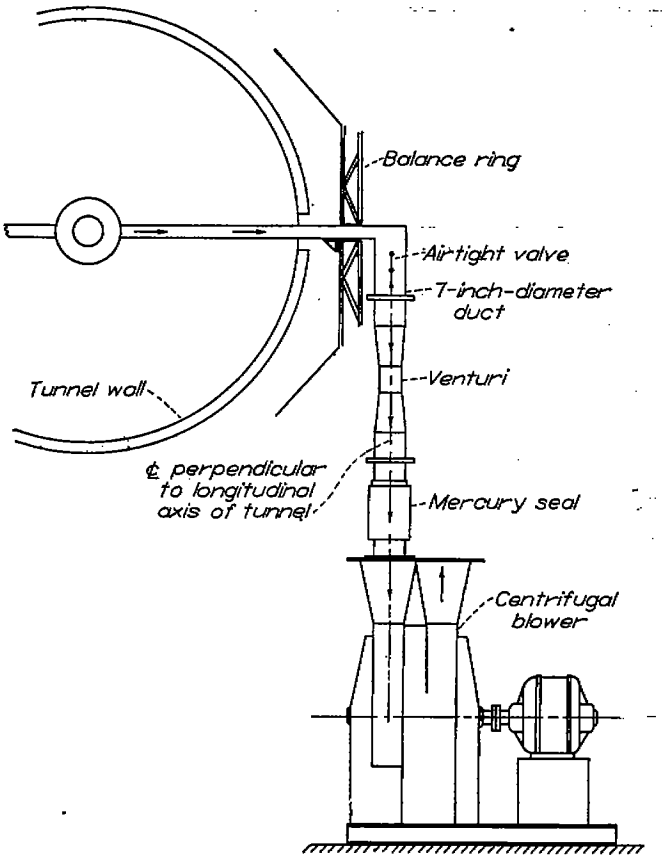

FIGURE 6.—Schematic diagram of setup for tests with blower.

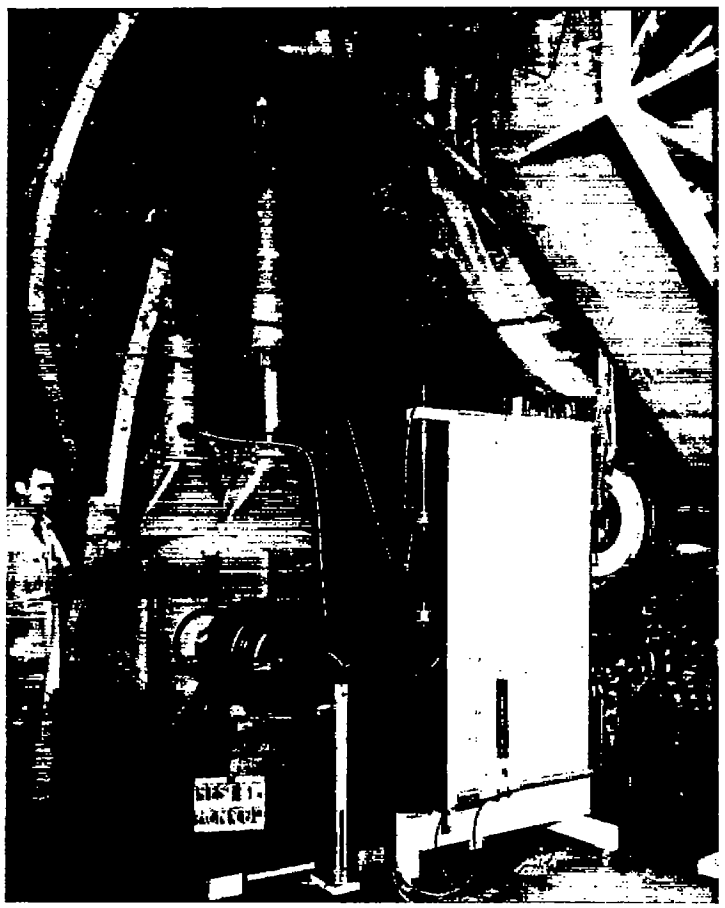

FIGURE 7.—General view of blower setup in the test chamber of the Langley 8-foot high-speed tunnel.

The flow in the system was controlled either by regulating the blower speed or by adjusting a butterfly valve. The zero flow condition was obtained by closing a special airtight valve located near the end of the wing duct. Utmost care was taken to prevent leakage in the system.

Inlet-outlet combinations.—The combinations tested and the internal-duct arrangement are shown in figure 1. The wing-duct openings within the body were faired over and sealed to prevent leakage. Flow regulation was accomplished by means of perforated plates of various conductance installed as shown in figure 2. Static-pressure orifices were installed at two stations in the converging section of the duct ahead of the outlet openings. The flow quantity was determined from the magnitude of the pressure drop between these stations according to a calibration obtained during the tests of the individual outlet openings with the blower-venturi setup. The total pressure and the static pressure at the outlet were determined from this same calibration. In several cases, as a check on the calibration, the quantities were measured directly by means of a small pitot-static tube mounted in the outlet opening.

No particular attempt was made to design an efficient internal-duct system because interest was centered on the external drag and because the blower was more than adequate to overcome large internal losses. However, in the combination tests with the duct open—that is, with no resistance plates inserted to restrict the flow—the internal losses were practically negligible owing to the low duct velocities.

Method of fixing boundary-layer transition.—Transition in the tests designated "with fixed transition" was fixed artificially by means of a ¼-inch wide ring of No. 180 carborundum grains glued to the surface at the desired station. It was found necessary to fix transition on the wing at the 10-percent station by the same method in order to make the drag of the wing constant so that the effective drag of the body could be obtained accurately.

Except for the strips of carborundum, the surfaces of the model were made aerodynamically smooth—that is, further conditioning would result in no decrease in drag.

Static-pressure measurement.—Flush orifices, closely spaced near the nose and in the vicinity of the openings, were installed along the top of the body. Additional static pressures on the bottom and on the side of the streamline body were obtained by means of a small movable static tube. The pressure tubing was led through a channel in the wing to a multiple-tube alcohol manometer in the test chamber.

Boundary-layer measurements.—The measurement of the boundary-layer profiles used in determining the transition point and in showing the effect on skin friction of air inlet was made with small survey units comprised of a single static and four total-pressure tubes. A discussion of the details of the method of determining the location of transition and a description of the small survey unit are given in reference 4.

Wake surveys.—In order to ascertain whether the drag-force measurements were affected by possible variations in the wind-tunnel pressure gradient due to air inlet at the nose, momentum-loss measurements were made in the wake behind the model with nose B. Vertical total-pressure-loss

profiles were obtained at 23 spanwise stations behind the wing and body at several rates of air inlet. The effective drag of the body was obtained by subtracting from the total drag of the section surveyed the drag of a corresponding section of the wing. The wake surveys were made only with nose B.

TESTS

The drag and the pressure-distribution measurements were made simultaneously. The transition determinations required a separate series of runs for each configuration.

Tests of the wing alone and of the wing with the streamline body were carried to 450 miles per hour. The tests of the openings were made at one speed only: 140 miles per hour. This speed was selected from considerations of the available blower performance and of the magnitude of the drag forces required for adequate precision.

The tests were made at an angle of attack of 0° (referred to the axis of the streamline body) with the exception of the runs with the gun in the inlet opening of nose B, which were carried to 3.5°.

RESULTS

The method of computing the velocity, the Mach number, and the Reynolds number in the Langley 8-foot high-speed tunnel is described in reference 5.

The drag data are presented in terms of the external-drag coefficient C_{D_F} plotted as a function of the internal-flow quantity coefficient $\rho Q/\rho_0 FV$. The external-drag coefficient represents the effective external drag of the body in the presence of the wing; the drag due to the internal flow was deducted from the measured effective body drag in all the tests.

The drag due to the internal flow arises from the change in the momentum of the flow in the drag direction. From the momentum equation,

$$\text{Drag force}=\text{Mass flow}\times(V_i-V_w)$$

where V_i and V_w are taken at the same static pressure and in the same direction as the air stream.

For the inlet-opening tests,

$$V_i=V$$

and

$$V_w=0$$

because the air was brought to rest in the drag direction. The drag-coefficient increment due to the internal flow therefore is

$$C_{D_{Fi_{inlet}}}=\frac{\rho QV}{q_0F}=2\left(\frac{\rho Q}{\rho_0FV}\right)$$

For the outlet-opening tests, the air exhausted through the outlets had no initial velocity in the drag direction—that is, $V_i=0$. The velocity at the exit opening v_e was necessarily measured where the static pressure p_e was generally different from the stream static pressure. Therefore the final outlet velocity attained at some distance behind the model where the pressure had returned to the free-stream static pressure p_0 was computed by Bernoulli's theorem

$$V_w=\left[v_e^2+\frac{2(p_e-p_0)}{\rho_0}\right]^{1/2}$$

and

$$C_{D_{Fi_{outlet}}}=-\frac{\rho Q}{q_0F}\left[v_e^2+\frac{2(p_e-p_0)}{\rho_0}\right]^{1/2}$$

or

$$C_{D_{Fi_{outlet}}}=-2\left(\frac{\rho Q}{\rho_0FV}\right)\left[\left(\frac{v_e}{V}\right)^2+\frac{(p_e-p_0)}{q_0}\right]^{1/2}$$

For the tests in which inlet-outlet combinations were investigated,

$$C_{D_{Fi_{combination}}}=C_{D_{Fi_{inlet}}}+C_{D_{Fi_{outlet}}}$$

whence

$$C_{D_{Fi_{combination}}}=2\left(\frac{\rho Q}{\rho_0FV}\right)\left\{1-\left[\left(\frac{v_e}{V}\right)^2+\frac{(p_e-p_0)}{q_0}\right]^{1/2}\right\}$$

or, in terms of the mean total-pressure loss in the duct ΔH,

$$C_{D_{Fi_{combination}}}=2\left(\frac{\rho Q}{\rho_0FV}\right)\left[1-\left(1-\frac{\Delta H}{q_0}\right)^{1/2}\right]$$

It will be observed from these equations that the large internal drag in the inlet tests and the thrust in the outlet tests are balanced in the combination tests, so that only a relatively small internal drag due to total-pressure losses in the duct occurs.

The internal flow quantity coefficient $\rho Q/\rho_0FV$ appearing in the equations is the ratio of the mass flow through the internal ducts to the mass flow at stream velocity through the area F, the maximum cross-sectional area of the body.

The pressure-distribution results obtained in the tests of the individual inlet and outlet openings are presented for a number of values of the ratio of mean velocity in the opening to stream velocity v/V. This parameter determines the local angle of attack at the inlet nose lip and hence governs the pressure distribution over a given nose shape.

The characteristics of the streamline body are shown in figures 8 to 11. Low-speed pressure-distribution data are given in figure 8, and the variation with Mach number of the peak pressure coefficients P_{max} on top of the body for the wing-body combination is presented in figure 9 with extrapolations to show the critical Mach number of the combination and of the body alone. The variation with Mach number of the critical pressure coefficient P_{cr}, the pressure coefficient corresponding to the local attainment of sonic velocity, is also shown in figure 9. Figure 10 shows the results of the transition measurements, and in figure 11 the force-test results, for Reynolds numbers ranging from 4,000,000 to 20,000,000 and the corresponding M values of 0.10 to 0.60 are given.

The results of the tests of the inlet openings with the inlet air exhausting through the external-blower system are presented in figures 12 to 21. Figure 12 shows the pressure distributions about the three inlet openings for various values of v/V (ratio of mean inlet velocity to stream velocity) compared with the streamline-body distribution. Only the

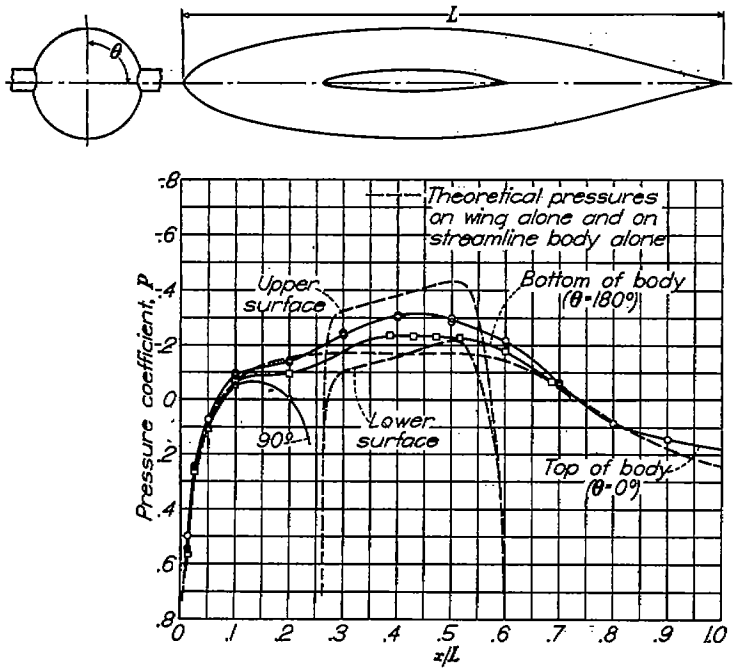

FIGURE 8.—Measured static-pressure distribution about streamline body mounted on NACA 27-212 airfoil compared with theoretical distribution on wing alone and body alone. $M=0.18$; $R=7.6\times10^6$.

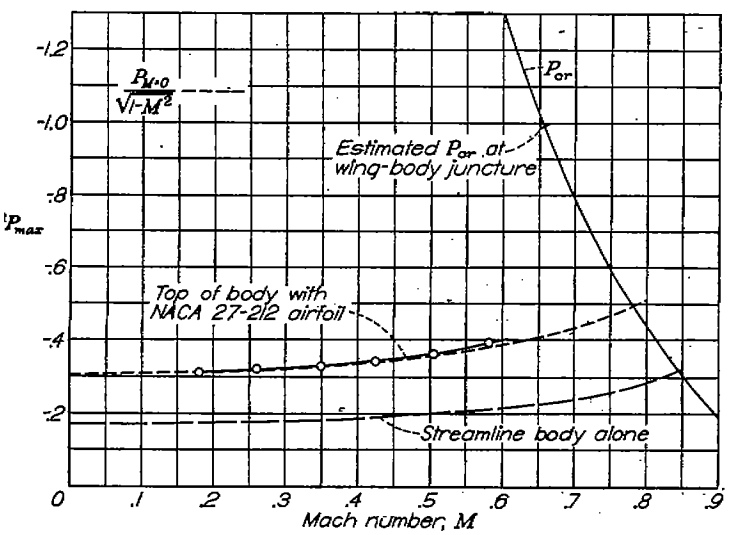

FIGURE 9.—Variation with Mach number of peak pressure coefficient on top of streamline body. Comparison with theory.

forward quarter of the body is represented because the pressures over the remainder of the body were essentially unaffected by the inlet openings. In figure 13 the pressure distributions on the bodies with noses A, B, and C and on the streamline body are compared at the condition of zero inlet flow and at a flow coefficient of 0.057, a practicable high-speed value. The inlet-velocity ratios corresponding to this flow coefficient are approximately 0.20, 0.40, and 0.80, respectively, for noses A, B, and C.

The drag and the transition results obtained are correlated in figure 14. Figure 15 shows the drag-force data obtained with transition artificially fixed near the leading edge of the noses as compared with that of the streamline body with transition fixed at corresponding locations. The drag obtained from the wake surveys is also plotted in figure 15.

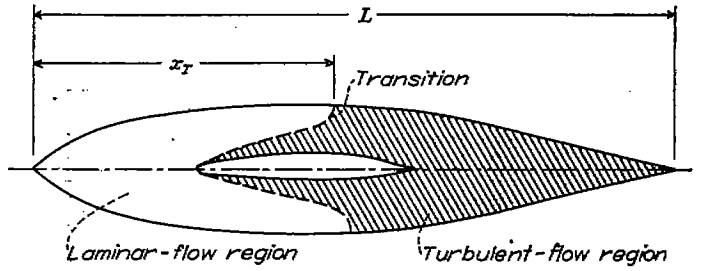

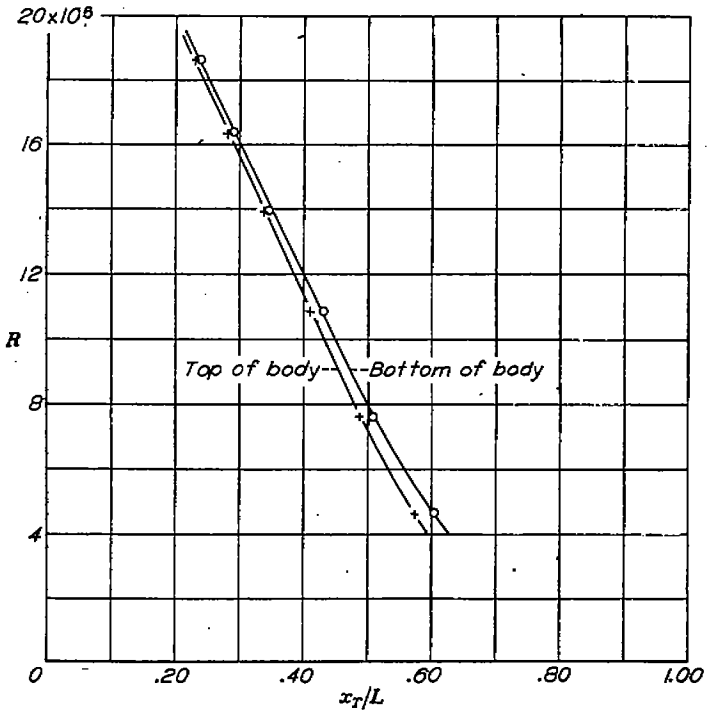

FIGURE 10.—Variation with Reynolds number of the location of the transition point on top and bottom of streamline body.

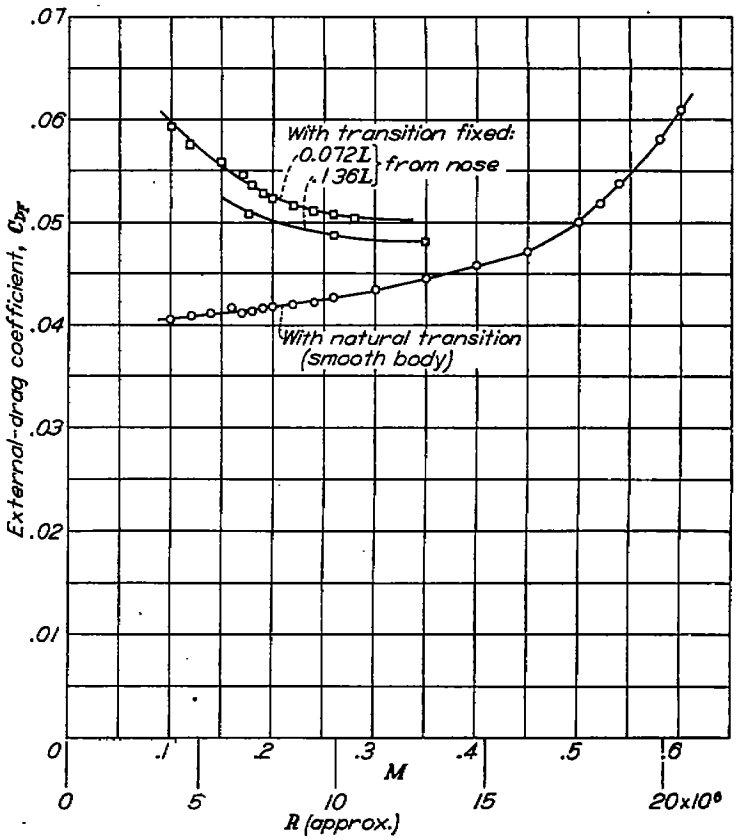

FIGURE 11.—The external-drag coefficient of the streamline body with fixed and with natural transition.

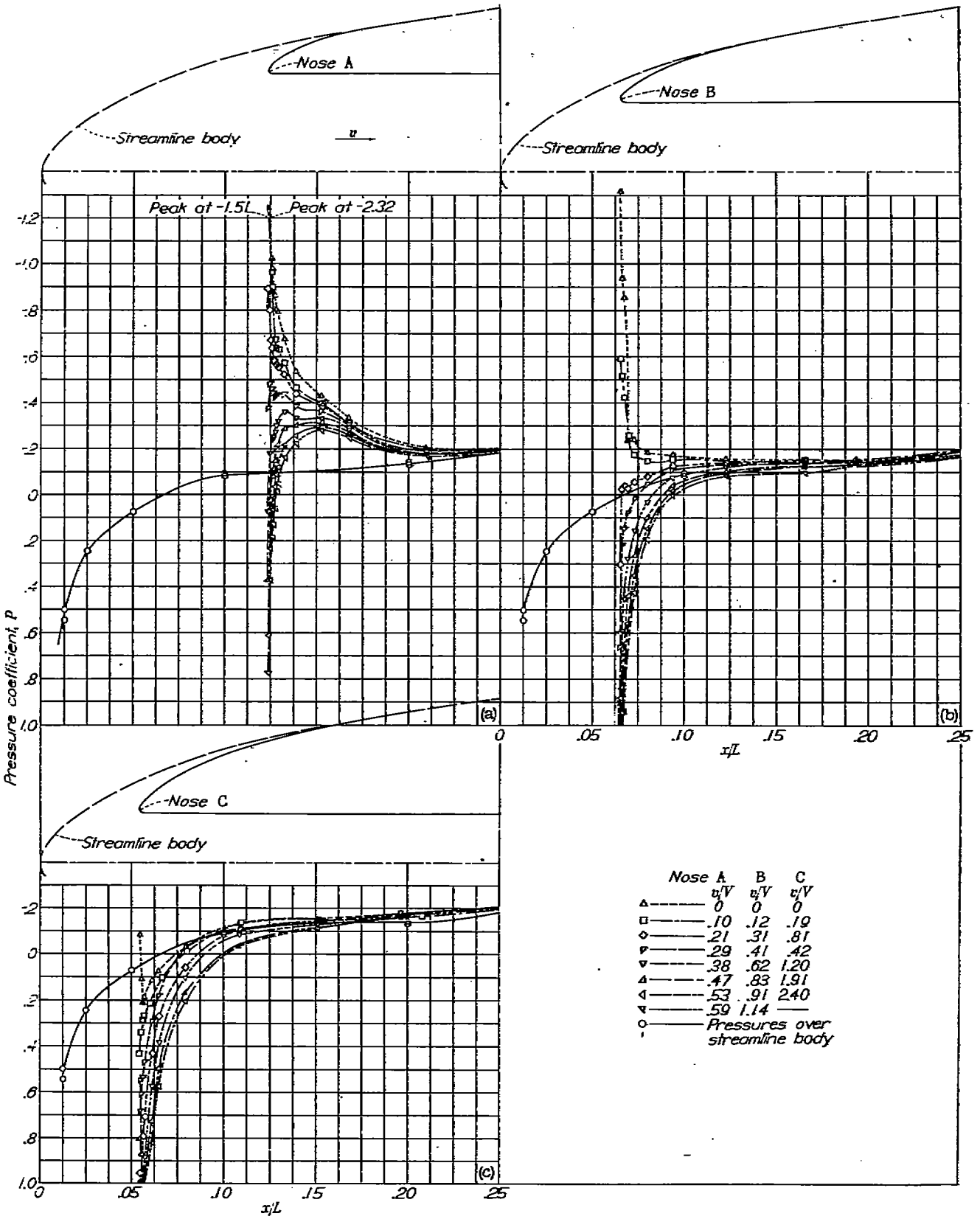

(a) Nose A. (b) Nose B.
(c) Nose C.

FIGURE 12.—The static-pressure distribution over the nose inlet openings.

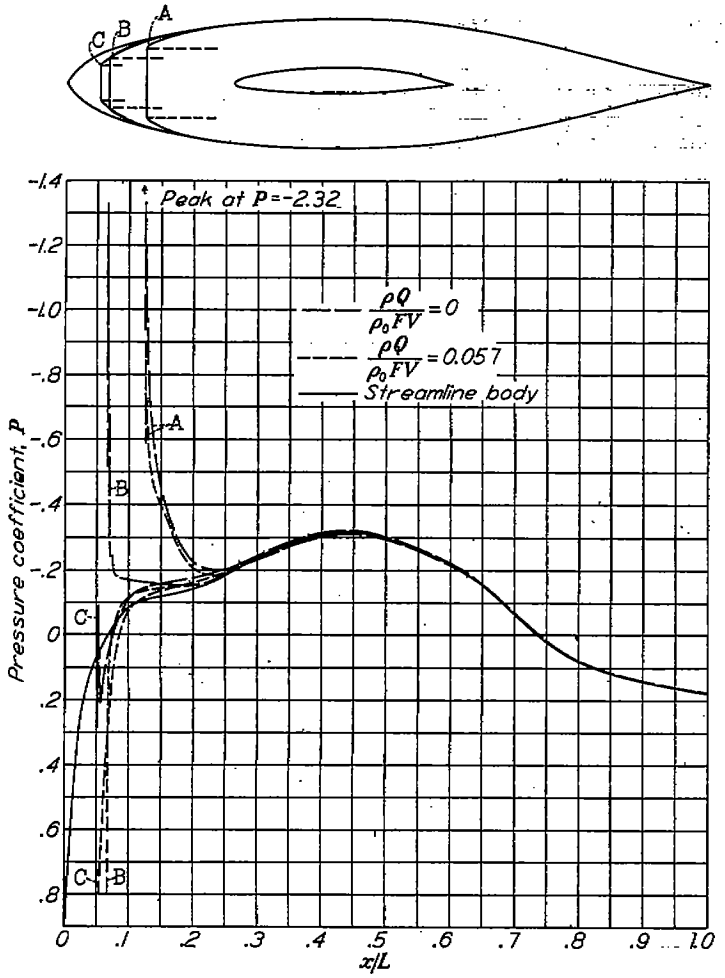

FIGURE 13.—Comparison of the static-pressure distribution over the three nose inlet openings at two rates of air inlet.

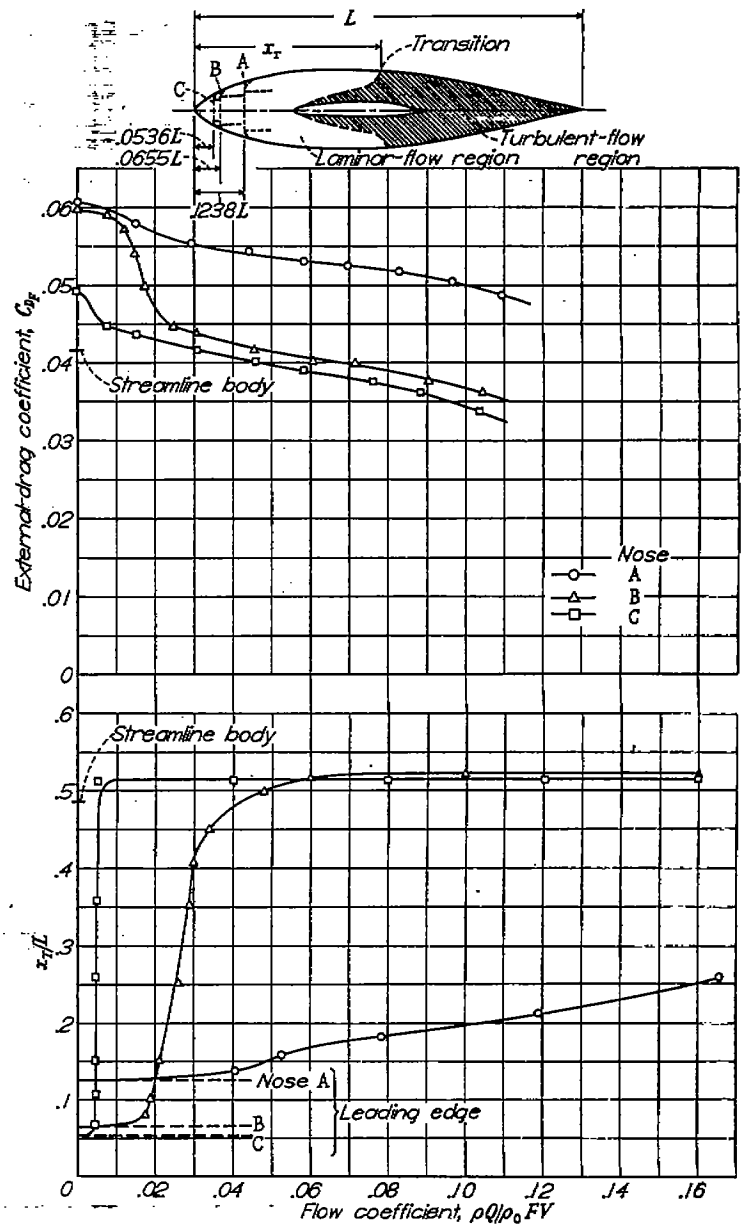

FIGURE 14.—Correlation of external-drag coefficient and transition-point location for the three nose inlet openings.

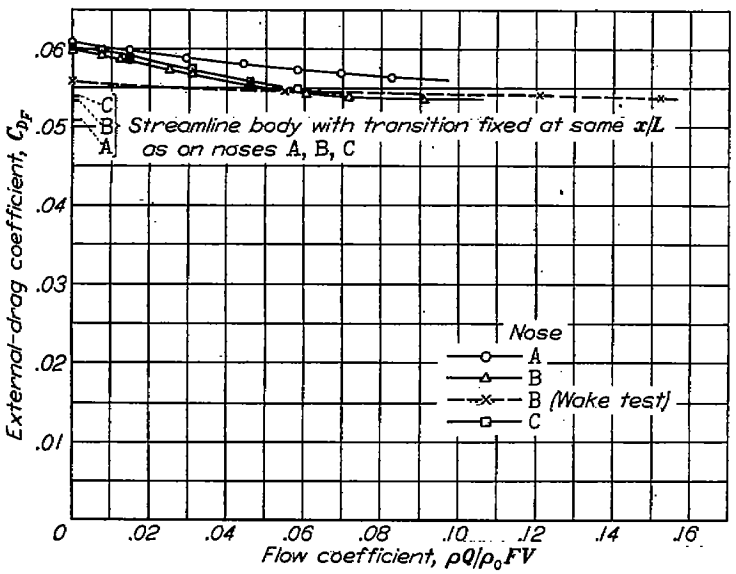

FIGURE 15.—The external-drag coefficient determined from both force and wake-survey tests with transition fixed at the nose of each inlet opening.

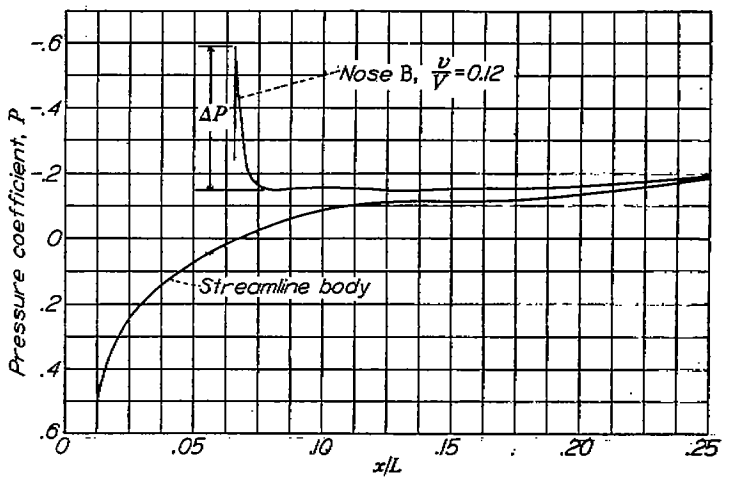

FIGURE 16.—Typical static-pressure distribution diagram for nose-inlet openings B and C at low rates of air inlet.

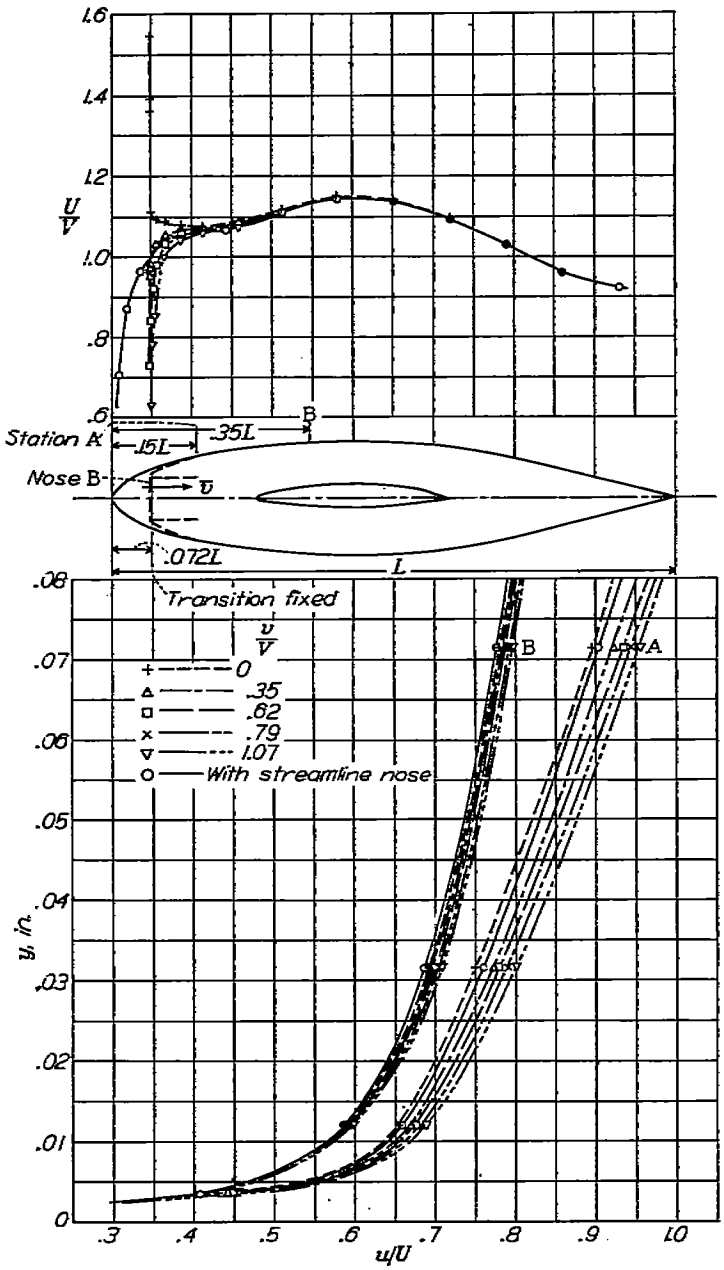

FIGURE 17.—Boundary-layer velocity profiles at two stations for various air-inlet velocity ratios, and the corresponding diagrams of local velocity distribution over the top of the body. Nose B; fixed transition.

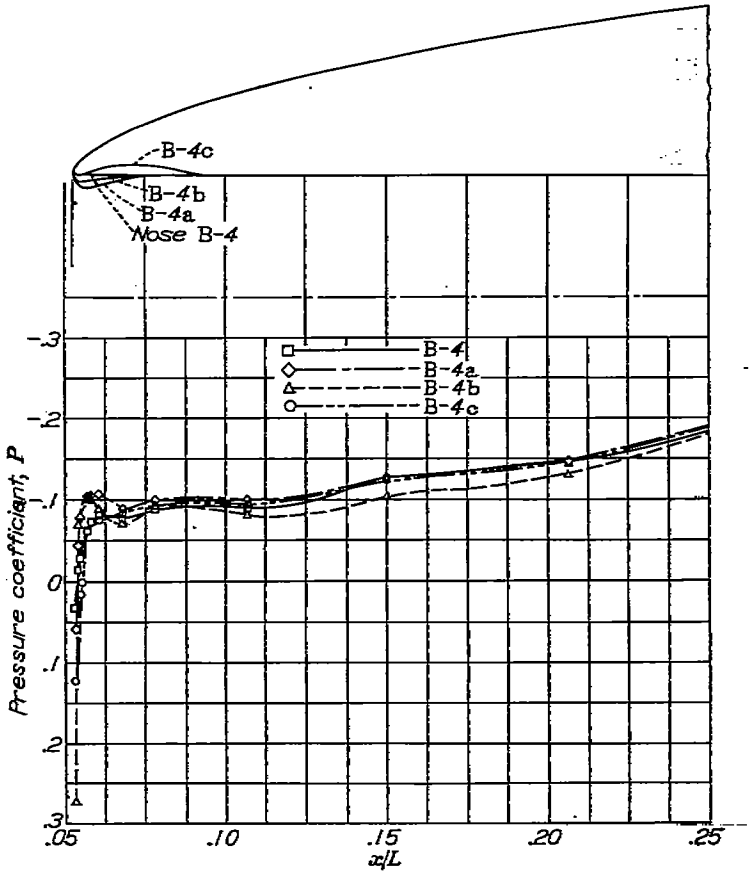

FIGURE 18.—The effect on static-pressure distribution of variations in nose shape at the duct entry. $\frac{v}{V}=0.30$.

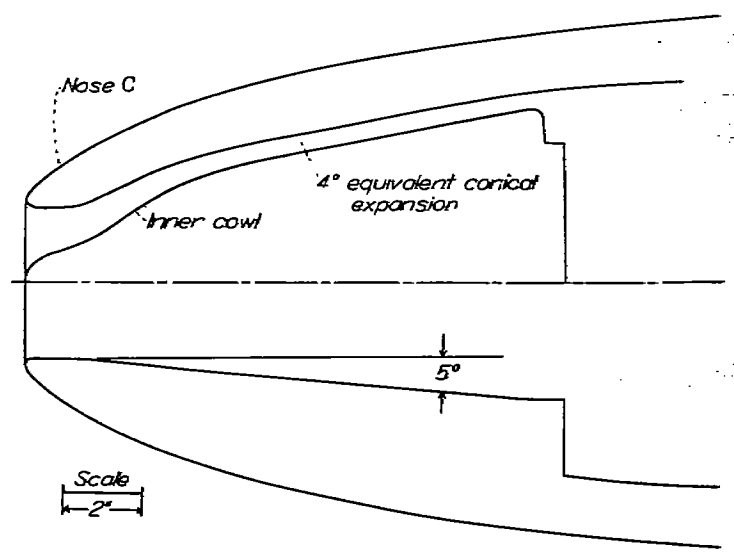

FIGURE 19.—Nose C with conical expanding duct and with inner cowl.

In the correlation of the pressure distribution and the transition data, it was found that for values of ΔP (fig. 16) greater than approximately 0.2, transition (fig. 14) occurred at the location of the pressure peak. For lower values of ΔP (higher rates of air inlet), extensive laminar boundary layers existed in spite of the large adverse pressure gradient that followed the peak.

The effect of air inflow (nose B) on the boundary-layer velocity profiles at two stations on the body is shown in figure 17.

In figure 18 the changes in pressure distribution resulting from modifications of the lip shape of nose inlet B–4 (one of the intermediate shapes tested in developing nose B) are given. The force-test results obtained with these modifications showed that shapes B–4a and B–4b caused very slight increases in external drag; the cut-out, B–4c, had no effect on the drag. Major changes in the internal duct employed with nose C (fig. 19) had no measurable effects on either the external pressure distribution or the external drag.

Optimum nose shapes for arbitrary inlet-duct sizes.—In order to make possible the derivation of optimum nose profiles for inlet-opening sizes other than those investigated, the three nose profiles tested were reduced to the same length

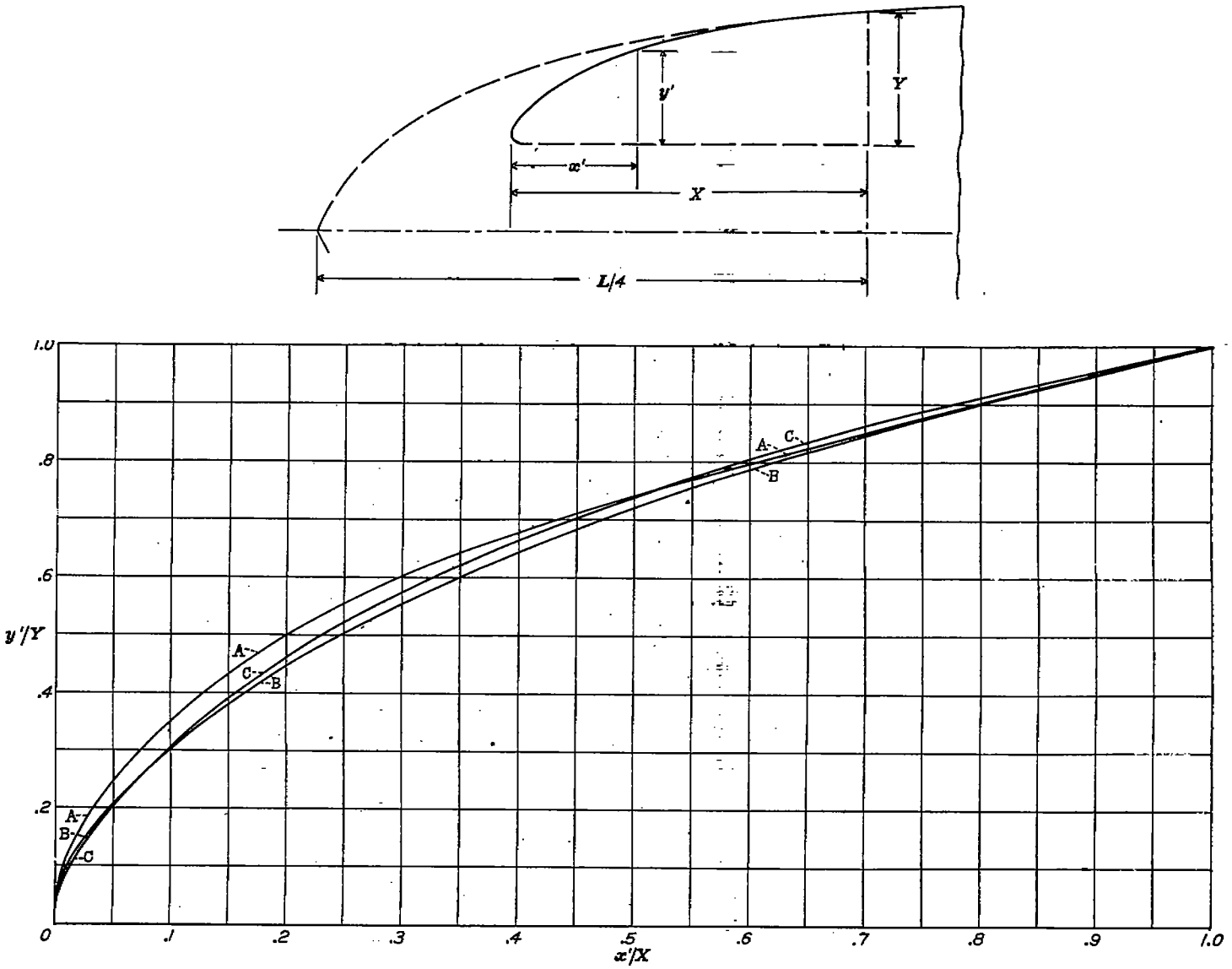

FIGURE 20.—Comparison of the three inlet-opening nose profiles reduced to the same length and depth.

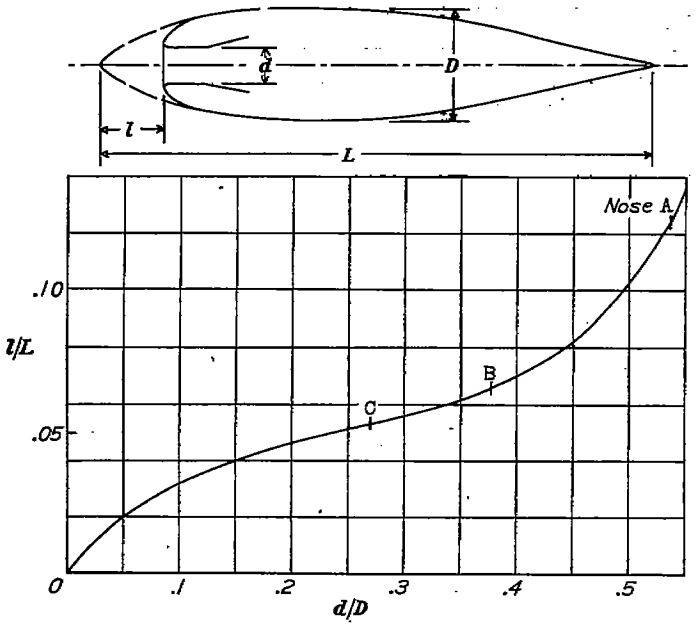

FIGURE 21.—Variation with duct diameter of the distance between the end of the nose and the tip of the streamline body.

(measured from the $L/4$ station of the streamline body) and the same depth. The ordinates thus obtained are given in table II and plotted in figure 20. The marked similarity of the profiles plotted in this way suggested that optimum nose shapes for intermediate inlet-opening sizes on the streamline body could be obtained either by interpolation or by the use of the mean of the three profiles of figure 20. The optimum nose length as a function of the inlet-opening diameter is given in figure 21. The actual nose-profile ordinates for a given inlet diameter are related to the nondimensional ordinates of figure 20 and table II as follows:

$$x'=\left(\frac{x'}{X}\right)X$$

or

$$x'=\left(\frac{x'}{X}\right)\left(\frac{L}{4}-l\right)$$

where l is obtained from figure 21. Similarly,

$$y'=\left(\frac{y'}{Y}\right)\left(y_{L/4}-\frac{d}{2}\right)$$

where $y_{L/4}$ is the ordinate of the streamline body at the quarter-length station. If desired, the nose ordinates referred to the end and center line of the streamline body (as in table I) may be obtained from the relations

$$\frac{x}{L}=\frac{x'}{L}+\frac{l}{L}$$

and

$$\frac{y}{R}=\frac{y'}{R}+\frac{d}{D}$$

or

$$\frac{x}{L}=\left(\frac{x'}{X}\right)\left(0.25-\frac{l}{L}\right)+\frac{l}{L}$$

and

$$\frac{y}{R}=\left(\frac{y'}{Y}\right)\left(0.90-\frac{d}{D}\right)+\frac{d}{D}$$

The results obtained in the tests of the outlet openings with air supplied by the blower are shown in figures 22 to 26. Figures 22 and 23 show the pressure and force-test results for outlets at the tail. Transition measurements with the largest tail outlet showed that transition occurred at the same station as on the streamline body (fig. 10). The pressure distribution obtained with the two annular outlets is shown in figure 24. Force-test results for the 63-percent annular outlet are given in figure 25. Transition measurements with the 21-percent annular outlet showed that transition occurred at the outlet for all rates of flow. The 63-percent annular outlet was about $0.14L$ behind the most rearward position of the transition point but appeared to have a slight influence on the transition location, such that the location was displaced somewhat toward the tail as the flow rate was increased.

Figure 26 shows a sketch of the probable outlet flow conditions with tail outlet D and with a suggested improved form of tail outlet.

Before the results of the inlet-outlet combination tests are presented, figure 27 is given in order to show the relatively small internal drag occurring in the combination tests. At high flow rates, where no internal resistance plate was required, this internal drag approached zero; whereas in the individual opening tests the internal drag was several times the external drag of the body. The external-drag determinations in the combination tests were consequently more reliable than in the tests of the single openings.

Figures 28 to 32 show the drag results obtained for the combinations of inlets with three tail outlets. Figure 33 compares the drag of the 63-percent annular outlet with that of tail outlet C when tested in combination with nose B.

The pressure-distribution results obtained with the combinations are not shown because no consistent measurable interference effects occurred—that is, the outlets had no appreciable effects on the pressures at the inlets and vice versa. Similarly, the transition locations on the combinations were the same as in the tests of the inlet openings alone.

In figure 34 the drag of the nose B and tail C combination is compared with an estimate of the drag based on the tests of the single openings. The drag increments (above the streamline-body drag) due to nose B and tail C were added to the streamline-body drag in making the estimate.

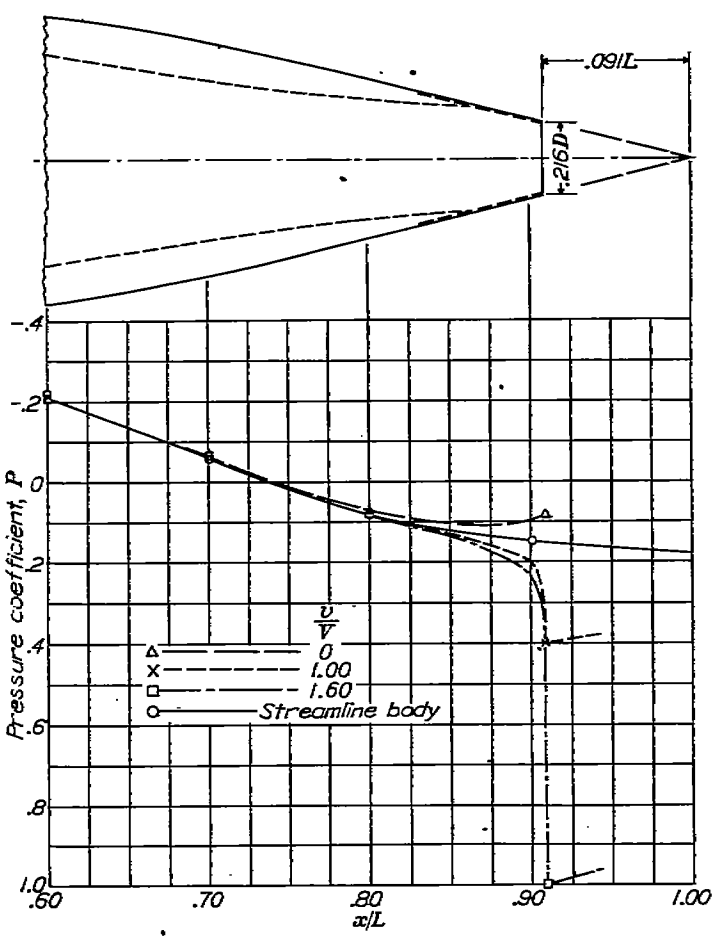

FIGURE 22.—The static-pressure distribution on the afterbody with a typical tail outlet. Tail D.

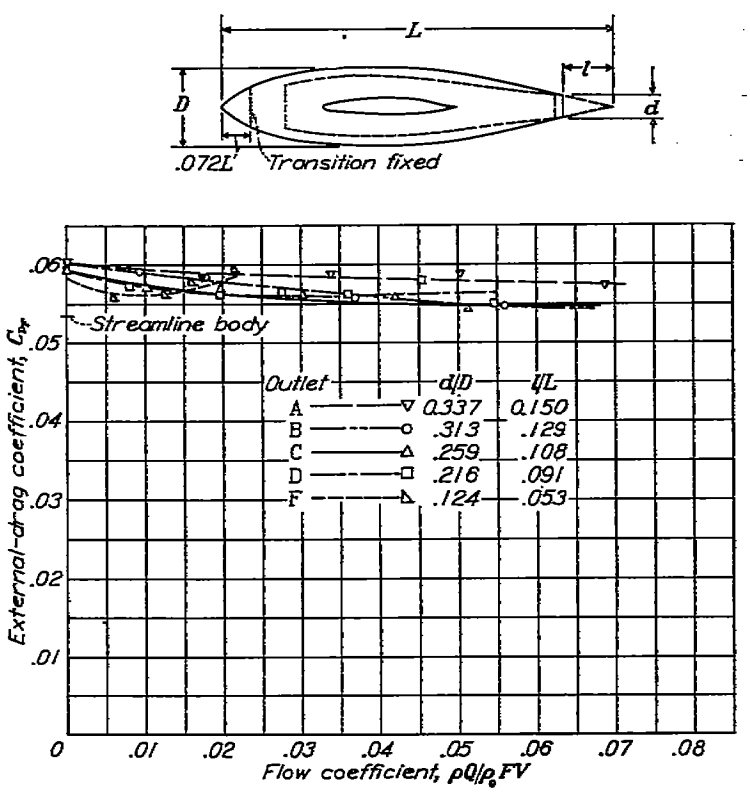

FIGURE 23.—Variation with flow coefficient of the external-drag coefficient obtained with the tail outlet openings. Fixed transition on nose.

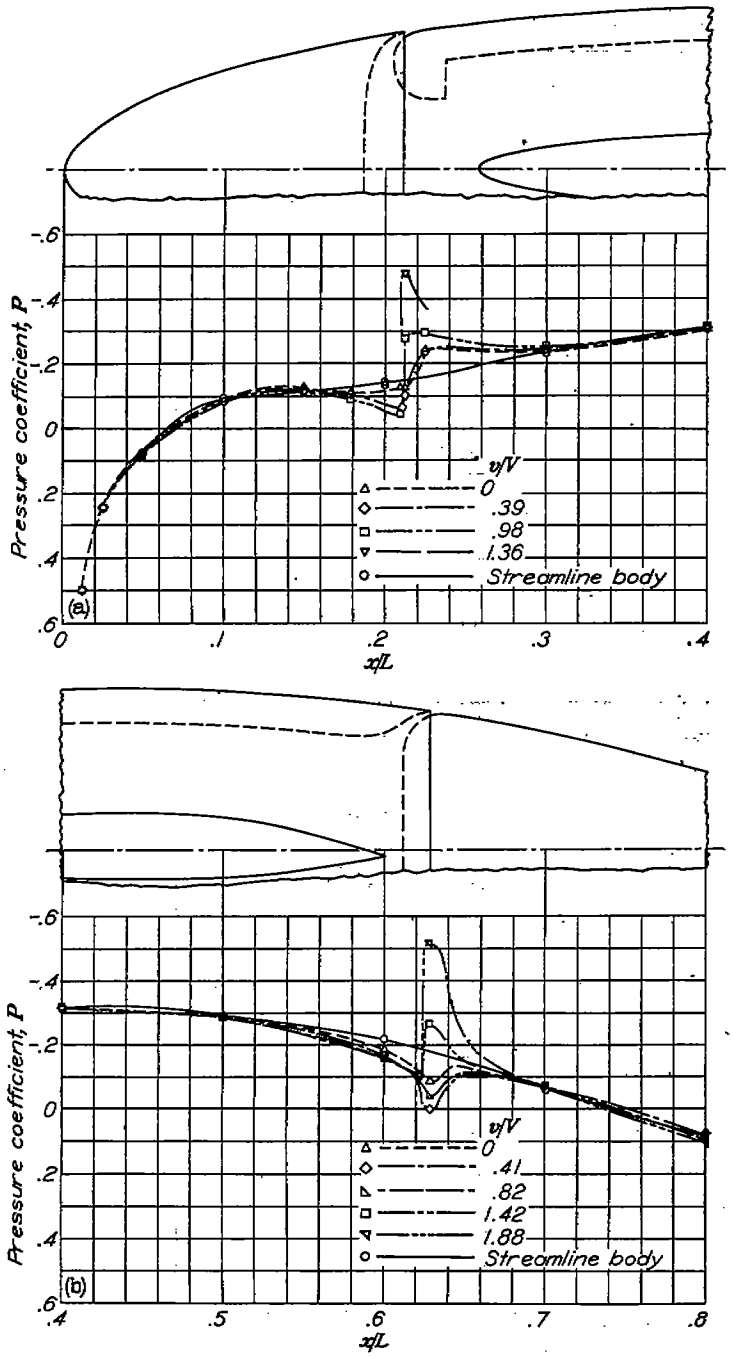

(a) Opening at 21-percent station.
(b) Opening at 63-percent station.

FIGURE 24.—The static-pressure distribution with annular outlet openings.

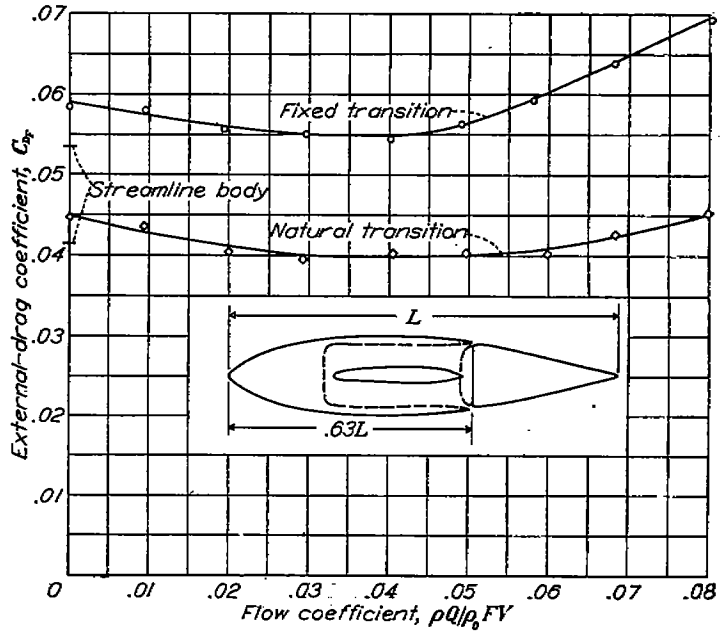

FIGURE 25.—Variation with flow coefficient of the external-drag coefficient obtained with the annular outlet opening at the 63-percent station.

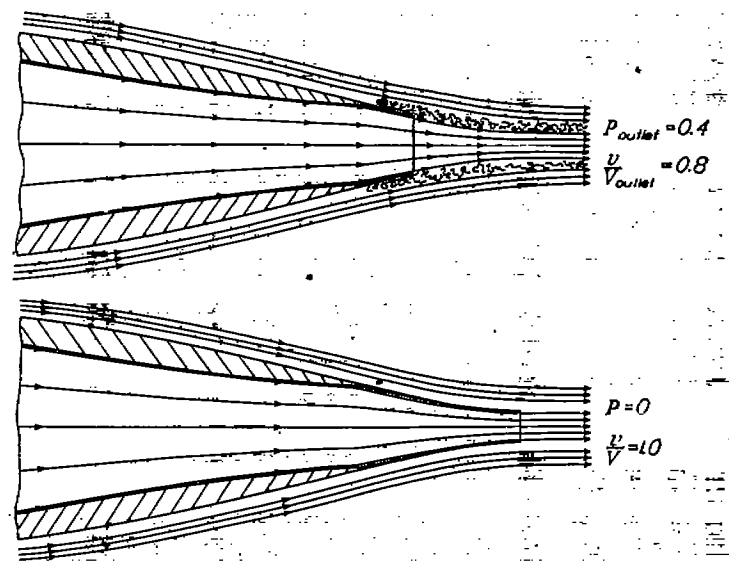

FIGURE 26.—Sketch of flow conditions (no internal losses) for a tail outlet opening, similar to those tested, and for a suggested improved type.

The main increase in drag due to the guns (table III) occurred at angles of attack other than zero as a result of partial separation of the external flow at the top of the nose as evidenced by the pressure-distribution plots (fig. 35). Increasing the rate of air inlet had a beneficial effect in reducing or preventing this separation. The smooth-barrel cannon had considerably less drag than the machine gun (sketched in fig. 35). Decreases in the length of the barrel extending beyond the nose resulted in appreciable drag reductions. It has been found that the drag of a smooth-barrel gun was considerably reduced by replacing the sharp edge at the muzzle of the gun with a rounded edge of small radius. It is considered likely that the unfavorable effects of the guns would be somewhat less in the high Reynolds number (fixed transition) condition than shown in table III, because no drag would result from disturbance of the laminar flow.

PRECISION

The accuracy of the body-drag determinations was somewhat impaired by the high drag of the wing with fixed transition relative to the body drag, the effective body drag varying from about 0.5 to 0.3 of the wing drag. In the tests of the individual openings, additional sources of error were the leakage of air in the external ducts and possible changes in the tunnel-pressure gradient due to the removal or the

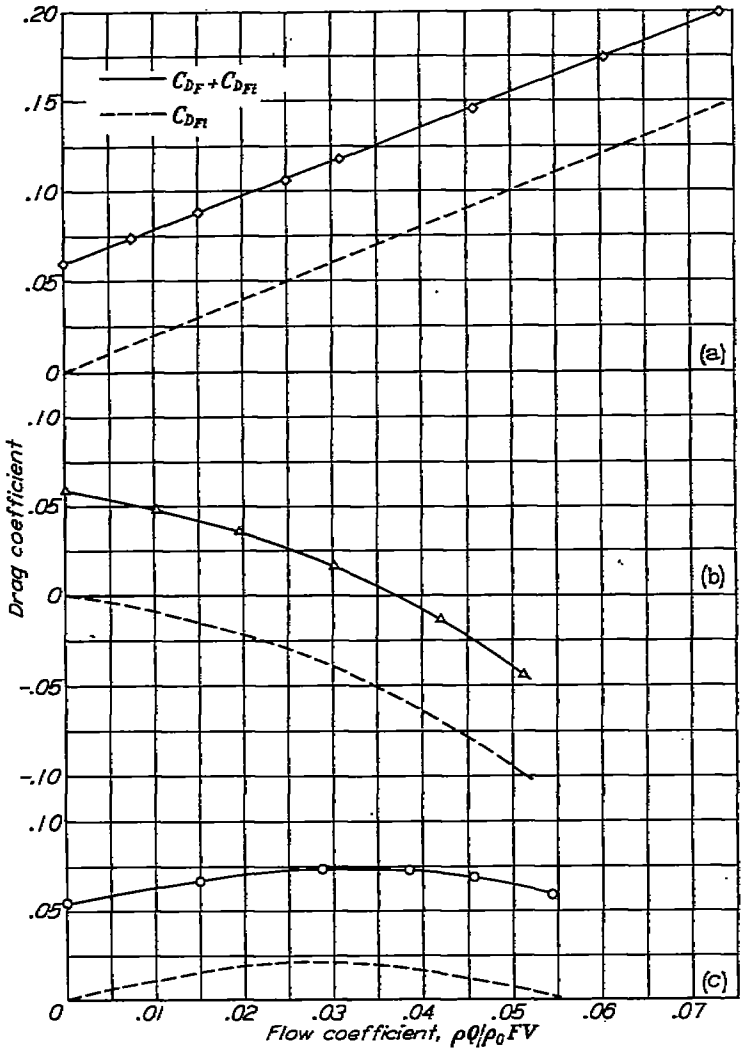

(a) Inlet: nose B; outlet: wing duct.
(b) Inlet: wing duct; outlet: tail C.
(c) Inlet: nose B; outlet: tail C.

FIGURE 27.—Comparison of magnitude of total body drag with internal drag in typical tests of individual openings and of a combination of an inlet and an outlet opening.

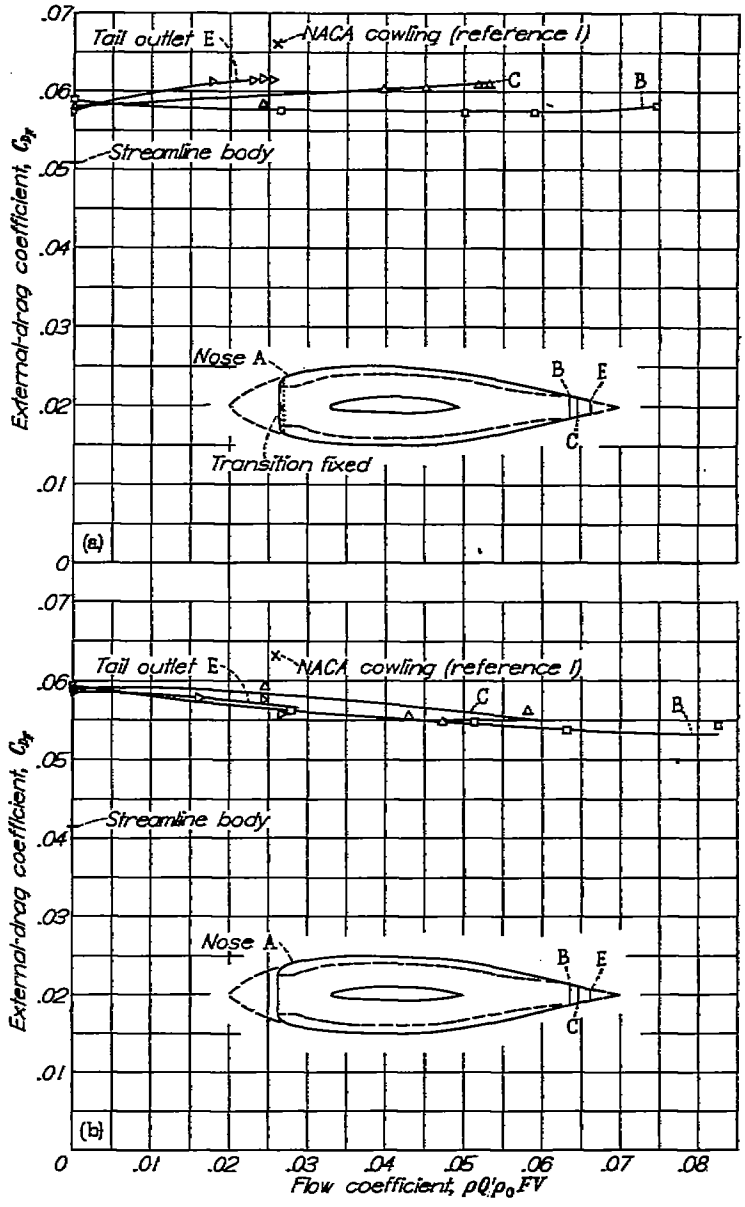

(a) Fixed transition.
(b) Natural transition.

FIGURE 28.—Variation with flow coefficient of the external-drag coefficients for nose inlet opening A combined with various tail outlet openings.

addition of air to the tunnel stream. The results obtained with the inlet-outlet combinations, however, are believed free of these two sources of inaccuracy because no air was added or removed from the tunnel and no leakage was likely due to the absence of all external ducts. A buoyancy correction of about 10 percent of the effective body drag was applied to all of the force-test results.

The wake measurements are more nearly free of these sources of error that affect the force tests. Evaluation of the possible magnitude of the drag-test errors will be made in the discussion of the results.

The precision of measurement of the rate of internal air flow is considered to be of a high enough order so that the external-drag determinations are practically unaffected by the small error in obtaining the internal drag, except possibly in the case of the individual opening tests at the highest rates of air flow. Repeated calibrations of the venturi during the tests showed excellent agreement.

The only significant sources of error in the pressure data are due to the inaccuracy of flow measurement and the tunnel-wall effects. The maximum possible change in the pressure coefficients due to the tunnel-wall effects was computed to be only about 3 percent. Possible errors in flow measurement could cause measurable changes in pressure coefficients only at the lowest inlet-velocity ratios.

DISCUSSION

STREAMLINE BODY

Pressure distribution and transition.—The presence of the wing had a pronounced effect on the pressure distribution over the body (fig. 8). The local velocities over the central portion were increased and the peak-pressure point was moved forward. At low Reynolds numbers the disturbances due to the wing controlled the location of transition on the body. (See sketch in fig. 10.) There was a rapid forward movement of the transition point with Reynolds number so

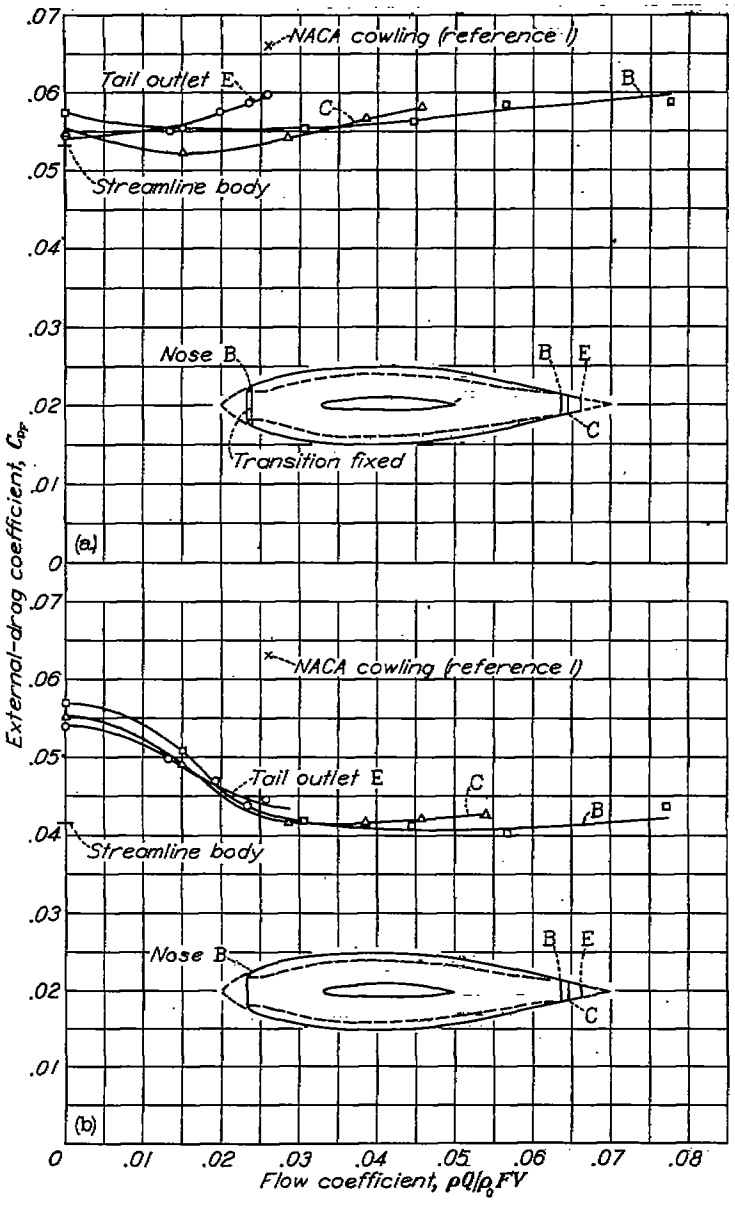

(a) Fixed transition.
(b) Natural transition.

FIGURE 29.—Variation with flow coefficient of the external-drag coefficients for nose inlet opening B combined with various tail outlet openings.

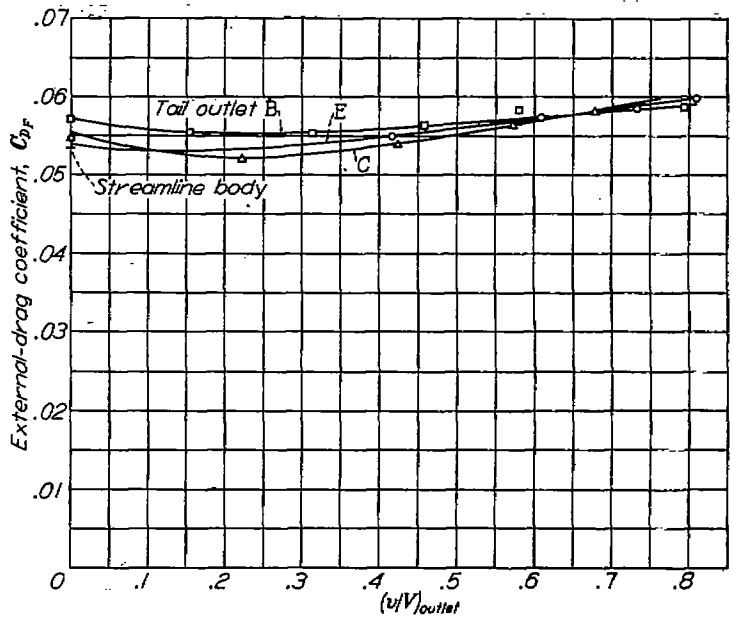

FIGURE 30.—Variation with outlet velocity ratio of the external-drag coefficients for nose B combined with various tail outlet openings. Fixed transition.

that at the highest test Reynolds number transition occurred considerably ahead of the leading edge of the wing (fig. 10). If a similar forward movement of transition with Reynolds number should occur under flight conditions, the extent of laminar flow obtainable at full-scale Reynolds number would be slight.

Critical speed.—The variation with the Mach number of the peak pressure coefficient on top of the body (fig. 9) was found to agree well with the theoretical variation (obtained from reference 6). Extrapolations of the low-speed, peak negative pressure coefficients to the critical pressure coefficient (at which the speed of sound is attained locally) were made according to the theory. The critical Mach number of the streamline body alone was thus found to be 0.84 (fig. 9), which corresponds to 600 miles per hour at 20,000 feet (−12° F) in standard air. The critical speed of a wing-body combination is considerably less than that of either component, owing to the increase in peak negative pressures on the wing due to the presence of the body. (See reference 6.)

Effective body drag.—Figure 11 shows the large differences in drag at low Reynolds numbers between the fixed and the natural transition conditions. Calculations based on flat-plate skin-friction coefficients showed that these differences are wholly accounted for by the changes in skin friction on the body. The difference decreases with increasing Reynolds number due to the forward movement of the transition point (fig. 10). The rise in the drag coefficient at the high Mach numbers is indicative of the approaching critical speed of the wing-body combination (estimated $M_{cr}=0.66$). Comparison of the magnitude of the low-speed drag coefficients with the results obtained in reference 3 for the NACA 111 form indicated that the flow over the body was satisfactory. Tuft surveys corroborated this conclusion. It was found, however, that the addition of the body to the wing caused a local separation of the flow at the trailing edge of the wing. The effective drag of the body was therefore somewhat higher than it would have been had a more efficient wing-body juncture been employed.

NOSE-INLET OPENINGS

Pressure distribution.—The nose-inlet shapes employed in this investigation were developed in a series of tests in which the nose shape and the length for a given inlet size were progressively modified to obtain the most satisfactory drag and pressure-distribution characteristics. It was found that by taking air into the body at sufficiently high velocities the

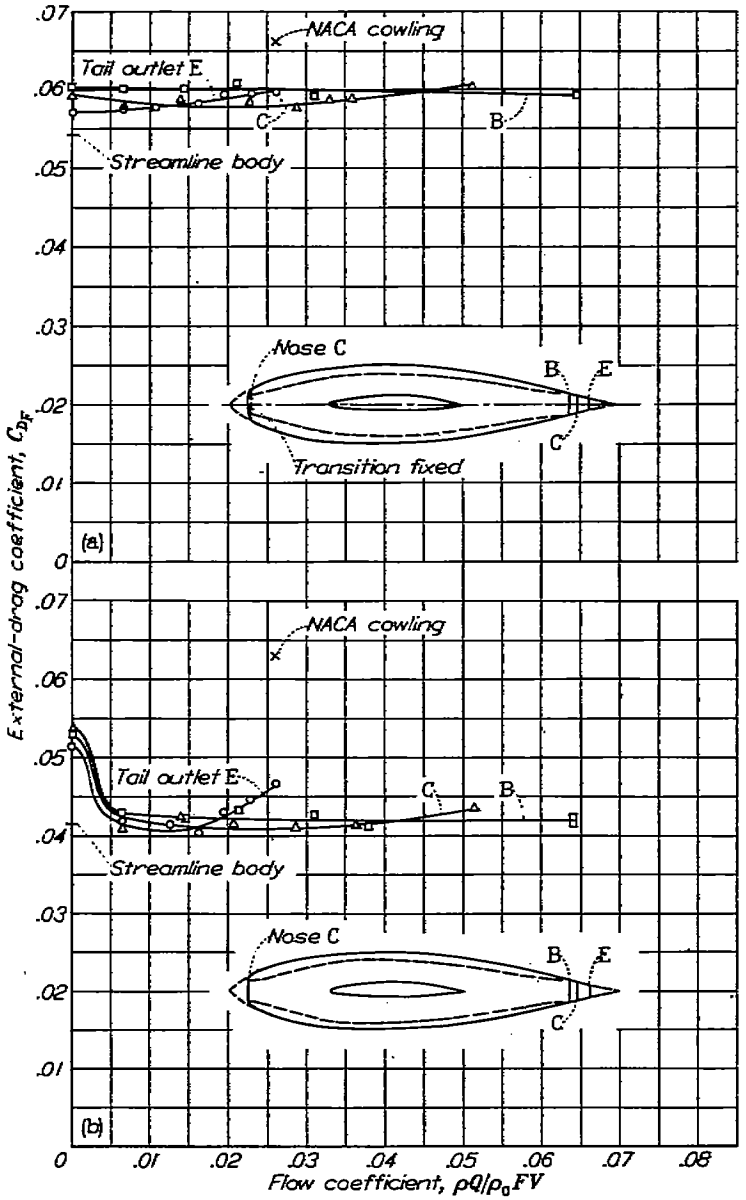

(a) Fixed transition.
(b) Natural transition.

FIGURE 31.—Variation with flow coefficient of the external-drag coefficients for nose inlet opening C combined with various tail outlet openings.

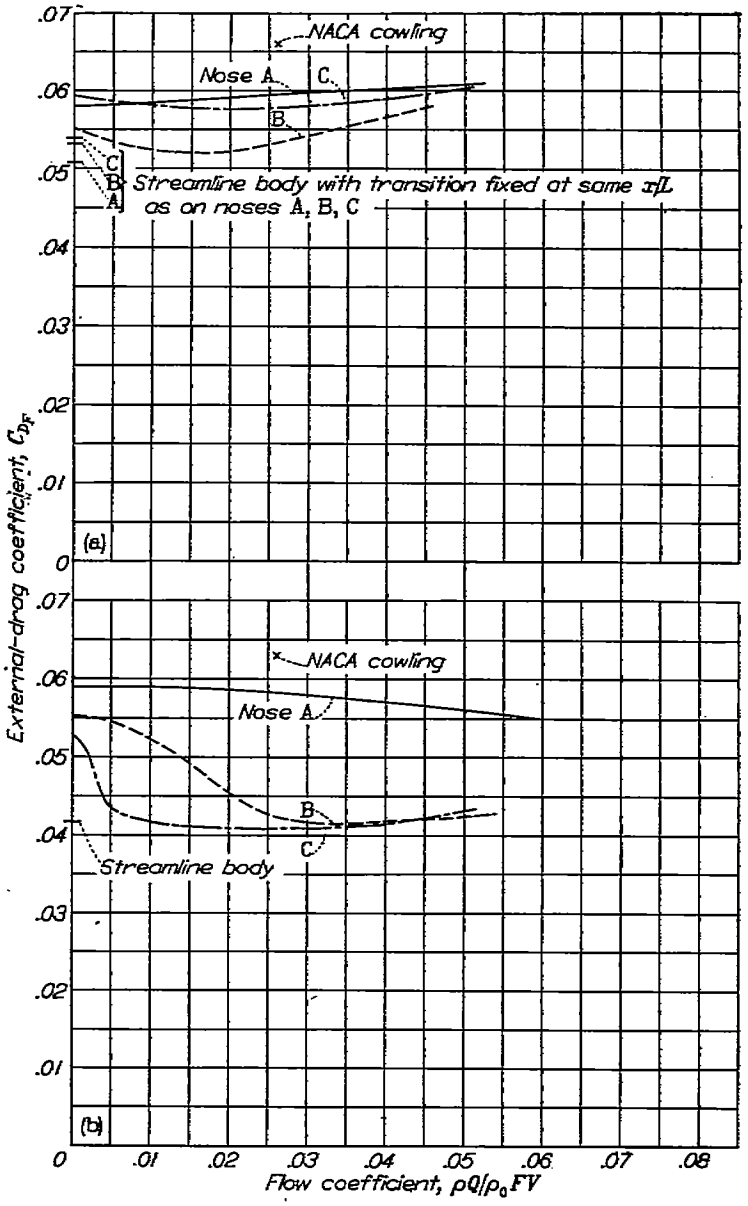

(a) Fixed transition.
(b) Natural transition.

FIGURE 32.—Comparison of the external-drag coefficients of the three nose-inlet openings tested with tail outlet opening C.

high negative-pressure peak which occurred over the noses at low flows could be greatly reduced in magnitude; for the smaller inlet sizes, the peak could be entirely eliminated. This result has the obvious beneficial effect of greatly increasing the critical compressibility speed which, as in the case of NACA cowling installations (reference 2), is generally fixed by the magnitude of the peak-negative pressures at the nose. In addition, it was found that laminar boundary layers as extensive as the ones with the streamline nose could be obtained. The design objectives then aimed at in developing noses B and C were to eliminate the pressure peak at as low an inlet-velocity ratio as possible and to obtain a uniform favorable pressure gradient similar to that of the streamline body. Figures 12 (b) and 12 (c) show that the desired results were achieved when the inlet-velocity ratios reached or exceeded 0.3 or 0.2 for noses B and C, respectively. Extensive laminar boundary layers (fig. 14) were formed even before the peak was fully eliminated with values of ΔP (fig. 16) as high as 0.2.

For the largest inlet opening, nose A, it was impossible entirely to eliminate the pressure peak, even with impractically high rates of air inlet (fig. 12 (a)). The peak was greatly reduced at practical inlet velocities but little advantage due to laminar flow was attainable (fig. 14).

Comparison of the pressure distribution of the streamline body with those for the three noses is made in figure 13 at a

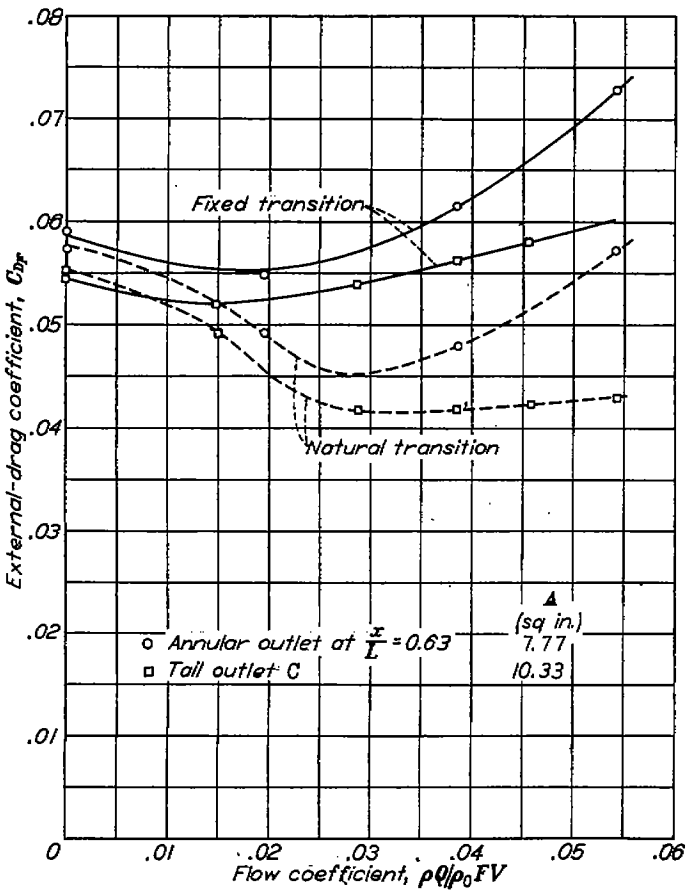

FIGURE 33.—Comparison of the external-drag coefficients of tail outlet C and the annular outlet at the 63-percent station of the fuselage. Nose B.

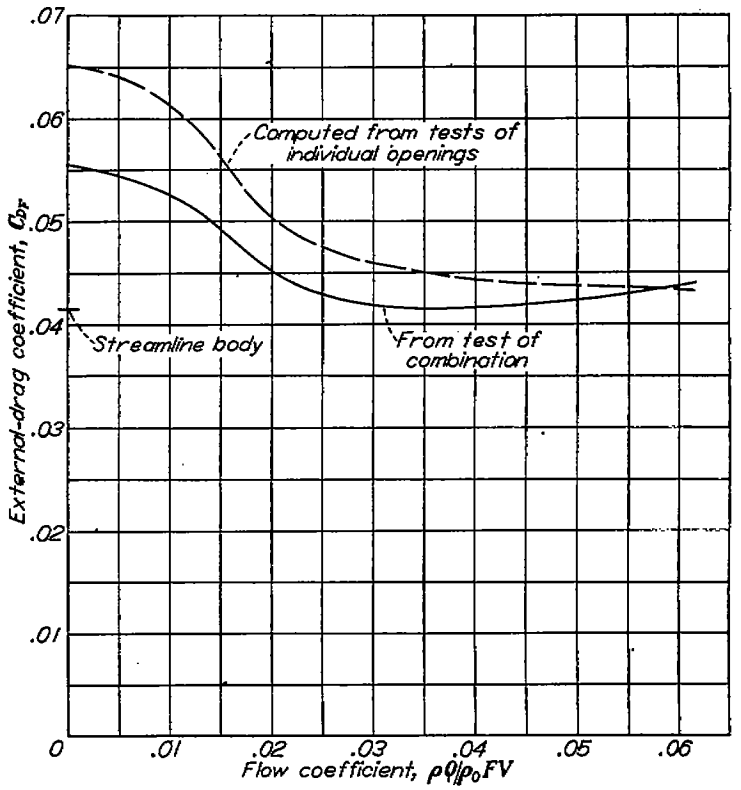

FIGURE 34.—The external-drag coefficient of the nose B and tail C combination compared with an estimate based on the drag increments obtained in the tests of the individual openings. Natural transition.

value of the flow coefficient corresponding to high-speed flight conditions and at zero flow.

Critical speeds.—The critical Mach number corresponding to the pressure peak on the largest inlet opening, nose A, at a practical rate of air inlet for a large radial engine (fig. 13), is 0.64. With the smaller inlets, noses B and C, no pressure peak occurred, and the indicated local velocity increments were so small that the critical speed of a fuselage employing these shapes would be determined by the cockpit enclosure or the wing-fuselage juncture—that is, the highest local velocity would occur at some point other than on the nose.

External drag.—Figure 14 shows that the abrupt decreases in external-drag coefficient of noses B and C at low rates of flow occurred as a consequence of the formation of extensive low-drag laminar boundary layers. This phenomenon did not occur with nose A because, as previously discussed, the unfavorable pressure distribution near the nose precluded the possibility of appreciable laminar flow. It will be noticed, however, that the drag of nose A showed a general decrease with increasing flow coefficient as did the drags of noses B and C after the laminar boundary layers had been formed. Similar decreases occurred with transition fixed (fig. 15).

In order to aid in finding the cause of the decrease in drag with increasing air-inlet velocity, partial boundary-layer velocity profiles were measured at two stations, $0.15L$ and $0.35L$, behind nose B with fixed transition for a wide range of inlet-flow ratios. The results (fig. 17) showed a decrease in the thickness of the turbulent boundary layer as the rate of air-inlet velocity was increased in spite of slight decreases in the velocity outside of the boundary layer. Two conclusions may be drawn from this result:

(1) The losses over the forward part of the nose are decreased as air inlet is increased.

(2) The skin friction over the main part of the body (to the rear of the $0.15L$ station) should increase slightly with air inlet.

From the drag results (fig. 15), it is evident that the decrease in losses at the nose more than compensates for the slight increases in skin friction behind the nose because an over-all decrease in external drag with air inlet occurs.

In regard to the magnitude of the external drag with air inlet, figure 14 shows that the external drag with noses B and C was reduced to less than that of the streamline body. For the fixed transition condition, the drag of these noses was approximately the same as for the streamline body. With nose A, in both cases, the drag was considerably higher. Tests of the three noses in combination with tail outlet C

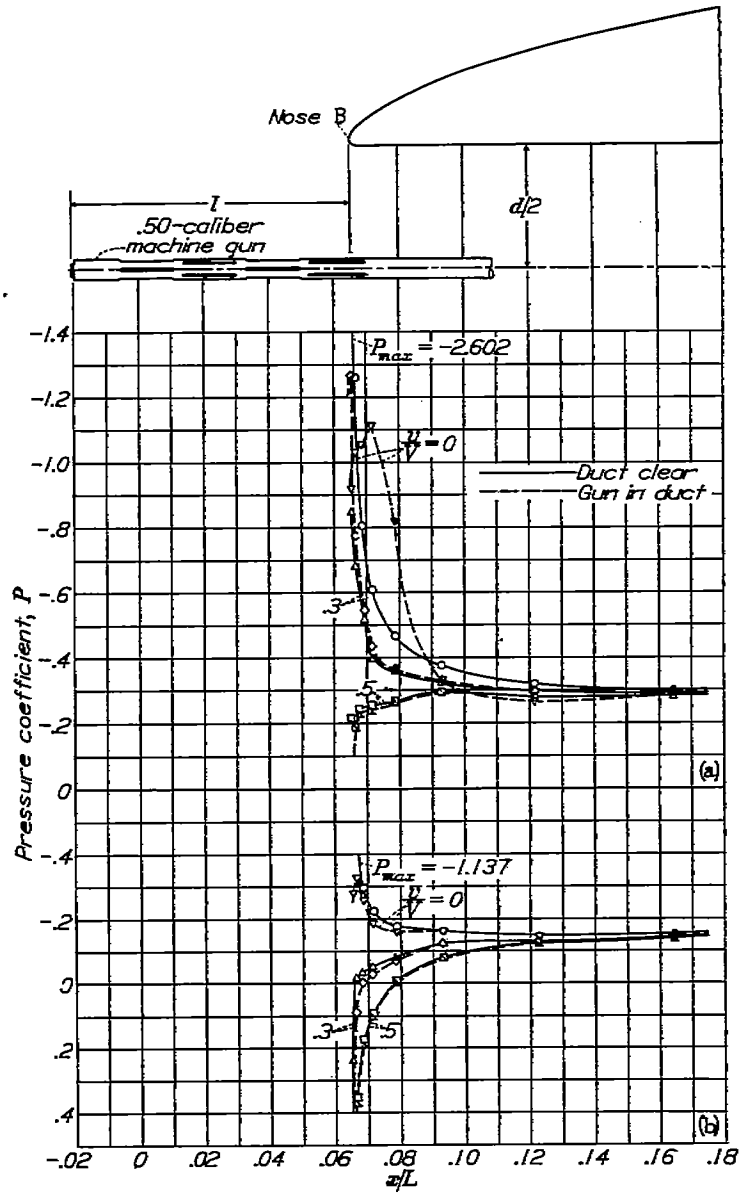

(a) α=3.5°.
(b) α=0°.

FIGURE 35.—The effect of the presence of a .50-caliber machine-gun model in the inlet opening on static-pressure distribution on top of the body. Nose B; natural transition.

(fig. 32) showed about the same relative drag characteristics as the tests of the single openings. The fact that the external drag with the openings decreased to that of the streamline body may be accounted for by the fact that the wetted area with the openings is somewhat less than that for the streamline body. In addition, the passage of air through the internal system has an effect on the external flow similar to a decrease in the effective thickness of the body.

The wake-survey results (fig. 15) show that the rate of drag decrease with air-inlet-flow coefficient was actually somewhat less than that indicated by the force-test results. The exaggerated effect shown by the force data is believed due to leakage and possible changes in the tunnel-pressure gradient as air was removed at the nose of the body. Maximum leakage would occur where the pressure in the duct system was the greatest and may account for part of the maximum discrepancy (7 percent) between force and wake drags occurring at zero flow, where stagnation pressure existed in the ducts. At a flow coefficient of about 0.11, the mean duct pressures, and hence leakage, reached a minimum; at this point the force and wake data agree closely. At least for the range of flow covered in figure 15, leakage effects apparently predominated over possible changes in the buoyancy effect in exaggerating the rate of drag decrease with air inlet.

Inlet-opening size.—The size of the inlet opening in an actual installation should be governed by considerations of both the external and internal flow. In a consideration of the external drag, it has been shown that nose B, although twice as large in area as nose C, was equally effective, so that either nose might be employed, the choice depending on the quantity of air flow required. It has also been shown that the opening must be designed for an inlet-velocity ratio of at least 0.3 in order to permit the nose-pressure peak to be eliminated. Higher inlet velocities would be of some benefit externally.

High inlet-velocity ratios are detrimental to the internal-duct efficiency because they necessitate large expansions and make the friction and bend losses high. It is suggested in reference 7 that low inlet velocities may have an additional advantage to the internal flow in that comparatively large expansions can be made efficiently near the inlet owing to the natural spreading of the streamlines at this point.

The final compromise between the conflicting requirements of the internal and the external flows will depend on the internal arrangement and the space available for the ducts. In general, it is believed that efficient installations incorporating nose B or nose C should have inlet-velocity ratios in the range of 0.3 to 0.6.

Derivation of optimum nose profiles for arbitrary inlet-opening sizes.—The method, described in section entitled "Results," for obtaining suitable nose-inlet shapes for inlet sizes other than those tested (see figs. 20 and 21) is obviously strictly applicable only to openings on the modified 111 body form. It was thought possible, however, that the shapes obtained by this method could be applied with good results where only the basic forebody profile was similar to the 111 body form. In a subsequent investigation (reference 8) it was found that considerable stretching of the nose B profile was permissible with the stretched profile still retaining the desirable flat pressure contour and low values of the pressure peak. It was thus indicated that the profile ordinates of the present tests could be directly used in the design of nose inlets having proportions greatly different from the shapes

developed in these tests. In order to simplify the procedure of designing inlets of other proportions, it was found desirable to base the nondimensional ordinates on the distance X from the maximum diameter station ($0.4L$) to the nose rather than on the distance from the $0.25L$ station to the nose, as suggested under "Results." Reference 9, which was an outgrowth of the present work, presents high-speed-test results for related inlets derived by the foregoing method and covers a wide range of proportions.

Internal-duct shape near inlet opening.—The modifications of figure 19 consisted of a conical expansion with a 10° included angle, a large irregular expansion formed by the cutout for the inner cowl, and a gradual (4° equivalent cone) annular expansion obtained with the inner cowl. None of these changes had a measurable effect on either the external drag or the pressure distribution. Modification B–4c of figure 18 likewise had no effects. Modifications B–4a and B–4b of figure 18, however, caused slight drag increases and disturbed the external pressures at the nose. These latter modifications are equivalent to inferior nose shapes corresponding to smaller inlet sizes than the basic nose B inlet. It will be observed that the internal-duct shapes included both satisfactory and very inefficient designs and that neither had any external effects, provided that the size of the inlet was not altered.

Angle of attack.—The effect of increase in angle of attack from 0° to 3.5° on the pressure distribution over the top of nose B can be seen in figure 35. A considerably higher air-inlet-velocity ratio is required to reduce the pressure peak at 3.5° angle of attack than at 0° angle of attack. In flight, the inlet-velocity ratio would automatically increase with angle-of-attack increases owing to decreases in the flight speed, if the engine power were assumed constant. Force-test data obtained with fixed transition on a fuselage model employing nose C (reference 8) showed that the external drag, at an inlet-velocity ratio of 0.56, was practically constant over the angle-of-attack range of 0° to 3.5°.

OUTLET OPENINGS

The outlet openings tested were not optimum shapes arrived at by a series of tests, as were the inlet openings. As previously stated, they merely represented typical practice in the design and the construction of outlets. It became apparent during the course of the tests that the openings had several undesirable characteristics, but it was not feasible at the time to extend the investigation to include modifications. Further outlet research embracing the improvements that suggested themselves in the course of this investigation are included in references 8 and 10.

Pressure distribution.—The effect on the pressure distribution of air flow from the outlets was generally unfavorable. In the case of the annular outlets (fig. 24) a negative-pressure peak occurred at the higher flow rates, owing to an effective thickening of the body due to the flow of exhaust air in the rear of the openings. In some cases, the peak was sufficiently high to fix the critical speed of the body. The pressure disturbance at the 21-percent outlet precipitated boundary-layer transition at all outlet velocities.

The static pressure at the tail outlets (fig. 22) became more positive as the flow was increased. This effect was due to the fact that the streamlines of both the internal and the external flows were converging at the opening, so that considerable contraction of the flow in the rear of the outlet resulted. Thus, about one-third of the total pressure (measured from p_0) at the tail outlets was in the form of static pressure which, of course, increased as the flow ratio was advanced. The static pressure in the internal flow at the outlet tended to be considerably more positive than that of the external flow near the tail outlet. The high outlet pressures are believed to have caused local separation of the external flow near the tail outlets.

External drag.—The external drag with the 63-percent annular outlet (fig. 25) at first decreased as the flow rate was advanced probably because of the elimination of locally separated flow in the wake of the opening, and then it increased rapidly, probably because of the increasing skin friction over the part of the body in the wake of the outlet.

Similar drag characteristics were exhibited by the tail outlets wherever velocity ratios v/V, up to 0.5 or greater, could be attained, as in the case of tails D and F tested singly (fig. 23) and tails B, C, and E tested in combination with the nose inlets (figs. 28 to 31). The rise in drag at the higher flow rates in the combination tests is shown conclusively in figure 30 to be due to the tail outlets. When compared on the basis of tail-outlet-velocity ratio (fig. 30) instead of flow coefficient (fig. 29 (a)), the drag obtained with three outlets of widely different size shows close agreement. The drag increase at the higher tail-outlet-velocity ratios is believed to be due to local separation of the external flow as a result of the high outlet pressures.

The tail outlets were superior to the annular outlets. A comparison of tail C with the 63-percent annular outlet in combination with nose B (fig. 33) shows that in spite of a somewhat larger area the tail outlet had the lower drag throughout the range, particularly at the higher outlet velocities. As would be expected, the comparison was independent of the location of boundary-layer transition because neither opening had any appreciable effect on the transition location.

Outlet-opening design.—The outlet velocity is not arbitrary as is the inlet velocity but is fixed by the internal total-pressure losses and the pressure drop across the system. From the standpoint of the internal drag, it is desirable to have the outlet total pressure as nearly equal to the free-stream total pressure as possible so that a minimum amount

of energy will be left in the wake. In well-designed cooling systems, the internal total-pressure losses are only a few percent of the free-stream total pressure at high speeds. Under these conditions, the ideal outlet total pressure is approached and the internal drag is small. The relation between internal total-pressure loss and the internal drag was shown in the section entitled "Results." The outlet velocity at a given flight speed is readily calculable from estimates of the total-pressure losses and the pressure drop across the system. A contraction or an orifice coefficient (dependent on the outlet shape) should be applied to the velocity as computed from the pressure characteristics. With the tail outlets tested, for example, the velocity at the outlet was about 0.8 of the final velocity. For the annular outlets, the coefficient was roughly 0.9. The velocity having thus been obtained at the outlet, the size of the opening will depend on the required quantity of air flow.

The economy of passing exactly the required amount of cooling air through the internal system at all flight speeds is generally appreciated. Variation in the size of the exit opening is the most efficient method of controlling the rate of flow.

The shape of the opening is not critical as far as the internal flow is concerned, provided there are no expansions. But the present tests have indicated that the external flow may be adversely affected if the static pressures are different from those of the main stream near the outlet. The shape of the opening, therefore, should permit the internal air to exhaust at the same static pressure as exists in the external flow near the opening. A suggested optimum tail-outlet shape is sketched in figure 26, and the flow characteristics are compared with those existing at one of the outlets tested for the ideal outlet condition of free-stream total pressure in the opening. The desired conditions at the outlet are obtained in the proposed opening by eliminating the contraction of the outlet flow. The desired outlet conditions can be attained at any outlet location by making the streamlines of both internal and external flows parallel.

The optimum shape for an annular-outlet opening is not as obvious as in the case of the tail outlets. It is evident from figure 24, however, that the body fairing immediately behind the outlet should be altered to reduce the thickness of the body and thus to relieve the thickening effect of the outlet flow. Further research is recommended to determine in detail the shapes required to give the minimum disturbance to the static-pressure distribution.

In regard to the relative merits of the annular and the tail outlets for efficient internal systems, it is probable that the optimum tail outlet will be superior to the best possible annular outlet because the high-velocity flow from the annular openings will generally increase the skin friction of the portion of the body in the wake of the outlet.

INLET-OUTLET COMBINATIONS

The combination tests (figs. 28 and 34) are of principal interest in showing that the over-all external drag of the body with suitable inlet and outlet openings of practicable size was no higher than that of the basic streamline form. This result was obtained at rates of internal air flow sufficient for cooling a radial engine located at the maximum fuselage section at moderate to high-speed flight conditions.

The variation of the rate of internal flow in the combination tests was accomplished by means of varying the internal resistance. At the condition of maximum flow attainable with a given outlet size, the internal losses were very small and consequently the outlet conditions closely approached the ideal. The outlet velocities over approximately the higher 25 percent of the flow range covered with each outlet correspond to high-speed-flight outlet conditions for typical heat-exchanger installations; at lower flow rates the internal-resistance losses were considerably higher than would be encountered in present practice. The actual magnitude of the internal drag throughout the flow range covered with tail C is shown in figure 27.

The rise in drag at the higher flow rates has been shown to be due to the unfavorable outlet conditions at the higher outlet velocities (fig. 30). It is believed that by improving the outlet design as suggested in figure 26 the rise in drag at the high outlet velocities would be eliminated.

It will be observed that the drag obtained for the best combinations with fixed transition was, in general, slightly greater than for the streamline body with transition fixed at the same station. The difference may be entirely accounted for by the higher drag of the carborundum strip itself when located at the nose of the inlet openings than when located in the thicker boundary layer on the streamline body. In addition, it should be remembered that the stations selected for fixing the transition on the streamline body are entirely arbitrary. Under actual flight conditions, transition on the streamline body might occur somewhat ahead of the corresponding station on the noses owing to the greater length of the streamline body. In this case, the drag of the streamline body would be relatively higher than in the present comparisons.

The drag of the inlet openings in the presence of the outlets, and vice versa, was considerably less than it was when the openings were tested individually. (See fig. 34.) A part of this effect, particularly at low rates of internal flow, may be due to leakage in the tests of the individual openings, as has previously been pointed out. Another contributing factor of secondary importance may be the difference in the methods of restricting the internal flow—that is, the resistance plates inserted near the inlet opening in the combination tests (fig. 2) may have had some small tendency to affect the external flow. In general, however, it is reasonable to expect

that the openings, in combination, would contribute less drag than when tested individually.

Comparison with NACA cowling.—The results of reference 1 provide a comparison of the inlet-outlet combinations with the NACA cowling. In the investigation cited, the best NACA cowling shape of reference 2 was adapted in a typical fuselage installation to the NACA 111 fuselage form. This basic streamline shape was almost identical with the body employed in the present tests, and the effective body-drag coefficients with natural and fixed transition, 0.040 and 0.055, respectively, were practically equal to the corresponding drag coefficients, 0.042 and 0.054, obtained in this investigation. The flow and the boundary-layer conditions on the basic shapes employed were evidently quite similar. The drags of the cowling with fixed and natural transition as given in reference 1, with cooling air flow, were reduced about 5 percent to obtain the external drag necessary to the comparison. The results, taken at the same Mach number and at very nearly the same Reynolds number as in the present tests, are shown on each of the figures along with the results of the combination tests (figs. 28, 29, and 31) with the tail outlets.

The combinations tested were aerodynamically superior to the NACA cowling, particularly in the natural transition condition where the inlets B and C permitted extensive laminar flow and caused no increase in drag. The NACA cowling produced a drag increase of some 56 percent in this case.

The NACA cowling shape employed in the tests of reference 1 was developed (reference 2) to have the highest critical speed, $M_{cr}=0.63$, of eight typical cowling shapes of the same over-all dimensions. The critical speed of the body alone with the largest of the present inlets, nose A, was $M_{cr}=0.64$ at a practical rate of air inlet (fig. 13). With the smaller inlets the critical speed was advanced to $M_{cr}=0.84$, the critical speed of the basic 111 fuselage shape.

CONCLUSIONS

The results of this investigation of inlet and outlet openings led to the following conclusions:

1. Modification of a streamline body permitting air inlet at the nose and outlet at the tail can be accomplished without increasing the external drag.

2. Inlet profiles were developed which, with practicable rates of air flow, produced velocity distributions approaching closely that of the basic streamline body. Consequently, the critical speed was as high as that of the streamline body and the same favorable laminar-boundary-layer-flow conditions were realized.

3. The test results indicated that outlet openings should be designed so that the static pressure of the internal flow at the outlet would be the same as the static pressure of the external flow in the vicinity of the opening.

4. The internal-duct shape near an inlet of given size had no appreciable effect on the external drag or pressure distribution.

5. The location of a simulated smooth-barrel gun in the nose-inlet opening caused no appreciable increase in drag at low angles of attack. The muzzle of the gun should be slightly rounded, and the length of barrel extending beyond the inlet should be as small as possible.

LANGLEY MEMORIAL AERONAUTICAL LABORATORY,
NATIONAL ADVISORY COMMITTEE FOR AERONAUTICS,
LANGLEY FIELD, VA., *September 11, 1940.*

REFERENCES

1. Draley, Eugene C.: High-Speed Drag Tests of Several Fuselage Shapes in Combination with a Wing. NACA ACR, Aug. 1940.
2. Robinson, Russell G., and Becker, John V.: High-Speed Tests of Conventional Radial-Engine Cowlings. NACA Rep. 745, 1942.
3. Abbott, Ira H.: Fuselage-Drag Tests in the Variable-Density Wind Tunnel: Streamline Bodies of Revolution, Fineness Ratio of 5. NACA TN 614, 1937.
4. Becker, John V.: Boundary-Layer Transition on the N.A.C.A. 0012 and 23012 Airfoils in the 8-Foot High-Speed Wind Tunnel. NACA ACR, Jan. 1940.
5. Hood, Manley J.: The Effects of Some Common Surface Irregularities on Wing Drag. NACA TN 695, 1939.
6. Robinson, Russell G., and Wright, Ray H.: Estimation of Critical Speeds of Airfoils and Streamline Bodies. NACA ACR, March 1940.
7. Patterson, G. N.: The Design of Aeroplane Ducts. Rules To Be Followed for the Reduction of Internal and External Drag. Aircraft Engineering, vol. XI, no. 125, July 1939, pp. 263–268.
8. Becker, John V., and Baals, Donald D.: Wind-Tunnel Tests of a Submerged-Engine Fuselage Design. NACA ACR, Oct. 1940.
9. Baals, Donald D., Smith, Norman F., and Wright, John B.: The Development and Application of High-Critical-Speed Nose Inlets. NACA Rep. 920, 1948.
10. Becker, John V., and Baals, Donald D.: High-Speed Tests of a Ducted Body with Various Air-Outlet Openings. NACA ACR, May 1942.

TABLE I

ORDINATES OF STREAMLINE BODY AND NOSE INLETS

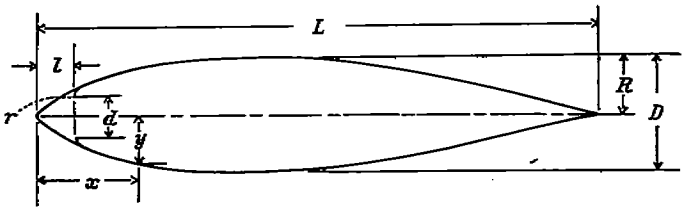

Streamline body			
x/L	y/R	x/L	y/R
0	0	0.5000	0.956
.0125	.190	.5500	.952
.0250	.287	.6000	.938
.0500	.431	.6500	.820
.0750	.536	.7000	.724
.1000	.620	.7500	.612
.1500	.742	.8000	.491
.2000	.826	.8500	.371
.2500	.893	.9000	.249
.3000	.948	.9500	.124
.3500	.982	.9750	.0624
.4000	1.000	1.0000	0
.4500	1.000		
$\frac{D}{L}=0.20$			

Nose A		Nose B		Nose C	
x/L	y/R	x/L	y/R	x/L	y/R
0.1238	0.550	0.0654	0.396	0.0536	0.286
.1244	.558	.0657	.408	.0540	.297
.1250	.578	.0660	.416	.0543	.304
.1258	.587	.0664	.420	.0546	.310
.1265	.595	.0668	.426	.0550	.317
.1272	.602	.0674	.432	.0557	.326
.1256	.614	.0682	.439	.0564	.334
.1300	.626	.0696	.451	.0578	.349
.1322	.640	.0724	.472	.0593	.361
.1358	.661	.0796	.516	.0607	.375
.1394	.680	.0868	.550	.0643	.404
.1465	.708	.0939	.580	.0678	.429
.1536	.732	.1082	.630	.0750	.478
.1608	.752	.1224	.670	.0822	.510
.1679	.768	.1368	.706	.0964	.574
.1822	.797	.1654	.768	.1107	.626
.1965	.821	.1939	.817	.1393	.707
.2108	.842	.2064	.837	.1678	.770
.2322	.875	.2321	.875	.1966	.821
.2500	.898	.2500	.898	.2322	.875
				.2500	.898
$\frac{r}{R}=0.0143$		$\frac{r}{R}=0.0143$		$\frac{r}{R}=0.0143$	
$\frac{l}{L}=0.1238$		$\frac{l}{L}=0.0653$		$\frac{l}{L}=0.0536$	
$\frac{d}{D}=0.5360$		$\frac{d}{D}=0.3785$		$\frac{d}{D}=0.2680$	

TABLE II

ORDINATES FOR DERIVING OPTIMUM NOSE SHAPES FOR INLET DUCT SIZES OTHER THAN THOSE TESTED *

x'/X	y'/Y			
	$\frac{d}{D}=0.536$	$\frac{d}{D}=0.379$	$\frac{d}{D}=0.268$	Mean
0	0.039	0.036	0.027	0.034
.005	.091	.079	.069	.080
.010	.119	.101	.089	.103
.020	.160	.135	.123	.139
.030	.192	.163	.152	.169
.050	.247	.211	.204	.221
.075	.303	.259	.268	.273
.100	.352	.304	.308	.321
.150	.435	.382	.392	.403
.200	.501	.448	.462	.470
.300	.603	.555	.574	.577
.400	.679	.644	.664	.662
.500	.740	.721	.740	.734
.600	.798	.788	.804	.797
.800	.902	.899	.910	.904
1.000	1.000	1.000	1.000	1.000

* See figure 20.

TABLE III

INCREASE IN DRAG WITH SIMULATED GUN IN NOSE-INLET OPENING

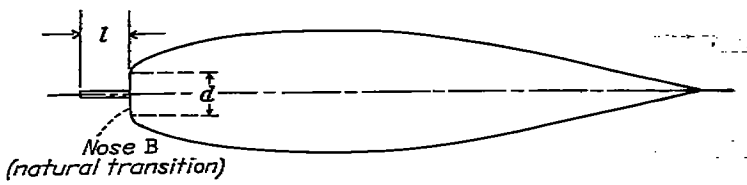

α (deg)	l/d	x/Y	Increase in body drag due to gun, percent
.50-caliber machine gun			
0	1.13	0	12.8
0	1.13	.25	12.5
0	1.13	.50	10.6
0	.57	0	9.6
0	0	0	2.6
1.5	1.13	0	21.5
1.5	1.13	.25	16.1
1.5	1.13	.50	10.2
3.5	1.13	0	33.6
3.5	1.13	.25	20.4
3.5	1.13	.50	7.2
3.5	.57	0	13.4
3.5	0	0	4.8
37-millimeter cannon (smooth barrel)			
0	1.13	0	6.7
0	1.13	.25	4.3
0	1.13	.50	0
1.5	1.13	0	11.5
1.5	1.13	.25	9.0
1.5	1.13	.50	0
3.5	1.13	0	19.2
3.5	1.13	.25	9.1
3.5	1.13	.50	0